Nonlinear Science 8 (2026) 100179

Contents lists available at ScienceDirect

Nonlinear Science

journal homepage: www.elsevier.com/locate/nls

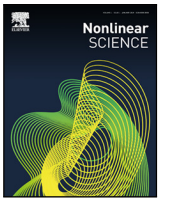

Research paper

Optimizing control strategies to reduce east coast fever spread in livestock–wildlife interface communities

Mirirai Chinyoka [a], Gift Muchatibaya [a], Mlyashimbi Helikumi [b], Shingirai T. Murambiwa [a], Prosper Jambwa [c], Steady Mushayabasa [a,d,*]

[a] Department of Mathematics and Computational Sciences, University of Zimbabwe, P.O. Box MP 167, Mount Pleasant, Harare, Zimbabwe
[b] Mbeya University of Science and Technology, Department of Mathematics and Statistics, College of Science and Technical Education, P.O. Box 131, Mbeya, Tanzania
[c] Department of Veterinary Biosciences, University of Zimbabwe, P.O. Box MP 167, Mount Pleasant, Harare, Zimbabwe
[d] Department of Mathematics, School of Engineering and Technology, Harare Institute of Technology, P. O. Box BE 277, Ganges Road, Belvedere, Harare, Zimbabwe

ARTICLE INFO

MSC:
34A34
34C23
92C60
92D30

Keywords:
East coast fever
Mathematical model
Cattle
Wildlife
Optimal control strategies

ABSTRACT

East Coast Fever (ECF) poses a significant threat to livestock in sub-Saharan Africa, leading to substantial economic losses primarily due to animal mortality. While buffalo are recognized as natural reservoirs of the disease, the role of the livestock–wildlife interface in the transmission dynamics of ECF remains poorly understood. To address this gap, a comprehensive mechanistic model incorporating this interface was developed, calibrated with empirical data collected from Zimbabwe between 2014 and 2020. Using this model, future ECF cases were projected up to the year 2030. Analysis of various control measures — including vaccination, acaricide use, and habitat management — indicates that, although these strategies can effectively reduce disease prevalence, they are unlikely to completely eradicate ECF within a single year when implemented individually. These findings underscore the importance of adopting integrated control approaches that combine multiple strategies, including biological methods, to achieve sustainable and long-term disease management. The results emphasize the need for continued research and coordinated efforts to effectively combat ECF and mitigate its impact on livestock and local economies in the region.

1. Introduction

East Coast fever (ECF), also known as theileriosis, is caused by protozoan parasites of the genus *Theileria*. It is a significant livestock pathogen capable of infecting multiple host species, including wildlife [1–3]. Despite extensive research over the past decade that has characterized the genotypic and antigenic diversity of *Theileria* [4–7], ECF remains a major challenge in sub-Saharan Africa. It is estimated that approximately one million cattle die annually due to ECF, with the mortality toll continuing since 1999 [8]. A key challenge in managing ECF effectively is the livestock–wildlife interface. Disease transmission at this interface is complicated by ecological processes that drive infection between wild reservoirs and sympatric livestock [9]. Understanding the dynamics of ECF in such communities is crucial for assessing local risks of transmission and persistence, yet this remains poorly understood.

* Corresponding author at: Department of Mathematics and Computational Sciences, University of Zimbabwe, P.O. Box MP 167, Mount Pleasant, Harare, Zimbabwe.
E-mail address: steadymushaya@gmail.com (S. Mushayabasa).

https://doi.org/10.1016/j.nls.2026.100179
Received 1 November 2025; Received in revised form 15 May 2026; Accepted 14 July 2026
Available online 20 July 2026

Mathematical models have been instrumental in exploring the mechanisms underlying ECF transmission (see, for example, [3,8,10–15]). These studies provide insights into factors influencing disease spread and evaluate intervention strategies. For example, Walker et al. [3] developed a model to assess acaricide use in communities at the livestock–wildlife interface, concluding that strategies targeting ticks and *T. parva* may not eradicate the disease. Gilioli et al. [10] used ODEs to analyze epidemiological processes, suggesting strategies such as integrated tick control and threshold-based interventions to establish enzootic stability. Mwambi et al. [13] proposed a stage-structured model highlighting the utility of control strategies in mitigating ECF spread. Recently, Chinyoka et al. [8] developed a mechanistic model of ECF that examines the effects of vaccination and acaricide use. Their findings suggest that acaricide alone, even at 80% effectiveness, may be insufficient to prevent transmission. However, combining acaricide with vaccination significantly reduces disease spread, and under certain conditions, elimination becomes feasible. These conclusions are supported by prior studies [16–18].

However, the impact of time-dependent control strategies on ECF at the livestock–wildlife interface remains under-explored. Optimal control (OC) theory offers a powerful framework for identifying the most effective strategies to minimize infectious agents at minimal cost over a specified period [19]. In this study, we aim to determine effective approaches to reduce ECF spread in such communities. We propose a mathematical model considering cattle and buffaloes as hosts and ticks as vectors. The model evaluates three control strategies: acaricide application, cattle vaccination, and pasture management (habitat modification). To our knowledge, minimal work has been done on the optimal control of ECF within a livestock–wildlife interface.

The remainder of this paper is organized as follows. In Section 2, we detail our methodology and results, including model formulation, calibration, prediction, and sensitivity analyses. We then extend the model to incorporate time-dependent controls aimed at optimizing resource use. Section 3 presents numerical simulations assessing the effectiveness of various strategies. Finally, Section 4 discusses key findings, limitations, and implications.

2. Methods and results

In this section, we develop a mathematical model of ECF transmission that incorporates livestock–wildlife interactions. We utilize a system of nonlinear ordinary differential equations.

2.1. Model formulation

This subsection presents the development of a mathematical model describing the transmission dynamics of ECF involving interactions between livestock and wildlife. The model employs a system of nonlinear ordinary differential equations (ODEs) to capture the complex interactions within and between host and vector populations. To investigate the transmission of ECF among ticks, cattle, and buffalo, we use a compartmental SIR-SI framework. The host populations are divided into susceptible ($S_i(t)$), infectious ($I_i(t)$), and recovered ($R_i(t)$) compartments, where $i = C$ (cattle) and $i = B$ (buffalo). The total host population at time t is given by $N_i(t) = S_i(t) + I_i(t) + R_i(t)$. The tick population is categorized into susceptible ($A_S(t)$) and infectious ($A_I(t)$) classes, with total tick population $N_T(t) = A_S(t) + A_I(t)$.

The model operates under the following assumptions:

(i) Populations of hosts and vectors mix uniformly within and across species, consistent with previous models of tick-borne diseases (e.g., [3]). Both clinically infected and recovered (carrier) animals can transmit ECF; however, recovered animals generally have a lower transmission rate than actively infected hosts [3]. Additionally, the disease is assumed to be fatal to clinically infected animals [3,15].

(ii) A susceptible cattle or buffalo becomes infected following a successful blood meal by an infected tick. The rate of this process is given by:

$$\lambda_{TC} = (1-p)\,\delta_C\,\beta_{TC}\,A_I, \tag{2.1}$$

$$\lambda_{TB} = p\,\delta_B\,\beta_{TB}\,A_I, \tag{2.2}$$

where β_{Ti} (for $i = C, B$) is the probability of transmission from an infectious tick to a susceptible host of species i, δ_i is the tick attachment (biting) rate for species i, and p is the proportion of blood meals taken on buffaloes. Consequently, $1-p$ is the proportion taken on cattle. These rates capture the likelihood of transmission events during tick-host interactions, accounting for host preferences.

(iii) A susceptible tick becomes infected after a successful blood meal from an infected host. The transmission rates are:

$$\lambda_{CT} = (1-p)\delta_C\beta_{CT}\left(I_C + (1-\eta_C)R_C\right), \tag{2.3}$$

$$\lambda_{BT} = p\delta_B\beta_{BT}\left(I_B + (1-\eta_B)R_B\right), \tag{2.4}$$

where β_{iT} (for $i = C, B$) is the probability of transmission from an infectious host i to a susceptible tick during a blood meal. The parameters η_i (for $i = C, B$) represent the transmission efficiency of recovered (carrier) hosts; specifically, $1-\eta_i$ indicates the reduced capacity of recovered hosts to transmit the disease compared to actively infected hosts.

Table 1
Model parameters and their biological definitions.

Sym.	Biological definition	Units	Sym.	Biological definition	Units
β_{TC}	Tick → cattle transmission rate	Month^{-1}	β_{TB}	Tick → buffalo transmission rate	Month^{-1}
β_{CT}	Cattle → tick transmission rate	Month^{-1}	β_{BT}	Buffalo → tick transmission rate	Month^{-1}
Π_C	Cattle recruitment rate	Month^{-1}	Π_B	Buffalo recruitment rate	Month^{-1}
η_C	Transmission efficiency of cattle carriers	–	η_B	Transmission efficiency of buffalo carriers	–
δ_C	attachment rate on cattle	–	δ_B	attachment rate on buffalo	–
μ_C	Natural mortality (cattle)	Month^{-1}	μ_B	Natural mortality (buffalo)	Month^{-1}
γ_C	Recovery rate (cattle)	Month^{-1}	γ_B	Recovery rate (buffalo)	Month^{-1}
d_C	ECF death rate (cattle)	Month^{-1}	d_B	ECF death rate (buffalo)	Month^{-1}
Π_T	Tick recruitment rate	Month^{-1}	μ_A	Tick mortality rate	Month^{-1}
p	Proportion of tick bites on buffalo	–			

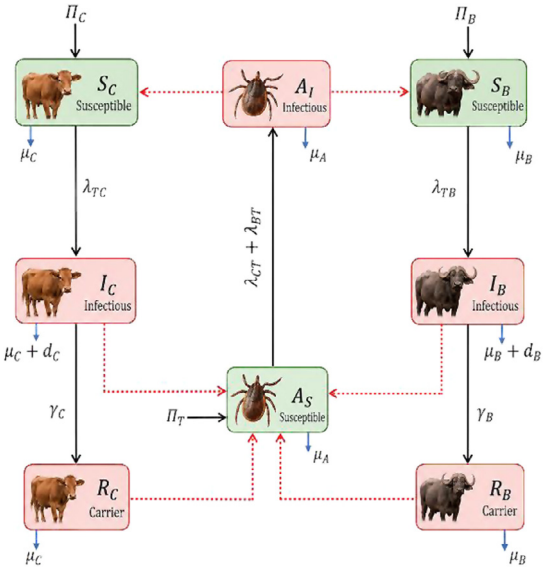

Fig. 1. Model flowchart depicting ECF transmission among cattle, buffaloes, and ticks. Host states include S_C (susceptible adult cattle), I_C (infectious cattle), R_C (recovered carrier cattle), and similarly for buffaloes: S_B, I_B, R_B. Tick states are A_S (susceptible adults ticks) and A_I (infectious adults ticks). Solid black lines represent transitions between states; red dashed lines indicate transmission between hosts and ticks.

Based on these assumptions, the system of differential equations governing the dynamics is as follows:

$$\begin{aligned}
S_C'(t) &= \Pi_C - \lambda_{TC} S_C - \mu_C S_C,\\
I_C'(t) &= \lambda_{TC} S_C - (\mu_C + \gamma_C + d_C) I_C,\\
R_C'(t) &= \gamma_C I_C - \mu_C R_C,\\
S_B'(t) &= \Pi_B - \lambda_{TB} S_B - \mu_B S_B,\\
I_B'(t) &= \lambda_{TB} S_B - (\mu_B + \gamma_B + d_B) I_B,\\
R_B'(t) &= \gamma_B I_B - \mu_B R_B,\\
A_S'(t) &= \Pi_T - (\lambda_{CT} + \lambda_{BT}) A_S - \mu_A A_S,\\
A_I'(t) &= (\lambda_{CT} + \lambda_{BT}) A_S - \mu_A A_I,
\end{aligned} \tag{2.5}$$

with initial conditions:

$$\begin{aligned}
&S_C(0) > 0, \quad I_C(0) > 0, \quad R_C(0) > 0, \quad S_B(0) > 0,\\
&I_B(0) > 0, \quad R_B(0) > 0, \quad A_S(0) > 0, \quad A_I(0) > 0.
\end{aligned}$$

Table 1 presents the model symbols (Sym.) along with their corresponding biological definitions. Additionally, the model flow diagram is depicted in Fig. 1.

It can easily be established that model (2.5) is epidemiologically and mathematically well-posed in the domain:

$$\Omega = \left\{ (S_C, I_C, R_C, S_B, I_B, R_B, A_S, A_I) \in \mathbb{R}_+^8, N_C \le \frac{\Pi_C}{\mu_C}, N_B \le \frac{\Pi_B}{\mu_B}; N_T \le \frac{\Pi_T}{\mu_A} \right\}. \tag{2.6}$$

2.2. The reproduction number

Since it quantifies the potential of an infectious disease to invade and spread within a population, the basic reproduction number, $\mathcal{R}_0$, remains a fundamental threshold parameter in infectious disease modeling. To compute $\mathcal{R}_0$, the disease-free equilibrium (DFE) must be identified. The DFE corresponds to a steady state where the disease is absent, characterized by $I_C = I_B = R_B = R_C = A_I = 0$. Under these conditions, the susceptible populations are at their equilibrium values:

$$S_C^0 = \frac{\Pi_C}{\mu_C}, \quad S_B^0 = \frac{\Pi_B}{\mu_B}, \quad \text{and} \quad A_S^0 = \frac{\Pi_T}{\mu_A}.$$

Using the next-generation matrix approach outlined in [20,21], the matrices $\mathcal{F}$ and $\mathcal{V}$ — which represent, respectively, the rates of new infections and the transfer/removal processes — are evaluated at the DFE:

$$\mathcal{F} = \begin{pmatrix} 0 & \frac{(1-p)\delta_C\beta_{CT}\Pi_T}{\mu_A} & \frac{(1-p)\delta_C\beta_{CT}(1-\eta_C)\Pi_T}{\mu_A} & \frac{p\delta_B\beta_{BT}\Pi_T}{\mu_A} & \frac{p\delta_B\beta_{BT}(1-\eta_B)\Pi_T}{\mu_A} \\ \frac{(1-p)\delta_C\beta_{TC}\Pi_C}{\mu_C} & 0 & 0 & 0 & 0 \\ 0 & 0 & 0 & 0 & 0 \\ \frac{p\delta_B\beta_{TB}\Pi_B}{\mu_B} & 0 & 0 & 0 & 0 \\ 0 & 0 & 0 & 0 & 0 \end{pmatrix},$$

and

$$\mathcal{V} = \begin{pmatrix} \mu_A & 0 & 0 & 0 & 0 \\ 0 & \gamma_C + \mu_C + d_C & 0 & 0 & 0 \\ 0 & -\gamma_C & \mu_C & 0 & 0 \\ 0 & 0 & 0 & \gamma_B + \mu_B + d_B & 0 \\ 0 & 0 & 0 & -\gamma_B & \mu_B \end{pmatrix}. \tag{2.7}$$

The spectral radius of the matrix $\mathcal{F}\mathcal{V}^{-1}$ yields the basic reproduction number:

$$\mathcal{R}_0 = \sqrt{\mathcal{R}_{0C} + \mathcal{R}_{0B}} = \sqrt{\begin{pmatrix}\text{Tick} \to \text{Cattle} \\ \text{Cattle} \to \text{Tick}\end{pmatrix} + \begin{pmatrix}\text{Tick} \to \text{Buffalo} \\ \text{Buffalo} \to \text{Tick}\end{pmatrix}}, \tag{2.8}$$

where:

$$\mathcal{R}_{0C} = \frac{(1-p)\delta_C\beta_{TC}\Pi_T}{\mu_A}\left[\frac{(1-p)\delta_C\beta_{CT}\Pi_C}{\mu_C}\left(\frac{1}{\mu_C+\gamma_C+d_C} + \frac{(1-\eta_C)\gamma_C}{\mu_C(\mu_C+\gamma_C+d_C)}\right)\right],$$

$$\mathcal{R}_{0B} = \frac{p\delta_B\beta_{TB}\Pi_T}{\mu_A}\left[\frac{p\delta_B\beta_{BT}\Pi_B}{\mu_B}\left(\frac{1}{\mu_B+\gamma_B+d_B} + \frac{(1-\eta_B)\gamma_B}{\mu_B(\mu_B+\gamma_B+d_B)}\right)\right].$$

- The terms $\frac{(1-p)\delta_C\beta_{TC}\Pi_T}{\mu_A}$ and $\frac{p\delta_B\beta_{TB}\Pi_T}{\mu_A}$ represent infection rates from ticks to cattle and buffalo, respectively. They reflect both tick density and transmission efficiency to each host species.
- The term $\frac{(1-p)\delta_C\beta_{CT}\Pi_C}{\mu_C}\left(\frac{1}{\mu_C+\gamma_C+d_C} + \frac{(1-\eta_C)\gamma_C}{\mu_C(\mu_C+\gamma_C+d_C)}\right)$ quantifies the expected number of ticks infected by a single infectious cattle. Carrier cattle dominate this term due to their longer infectious lifespan, despite transmitting less efficiently per bite. Here, β_{CT} is the probability a susceptible tick becomes infected after feeding on infectious or carrier cattle. The duration of acute infectiousness is given by $\frac{1}{\mu_C+\gamma_C+d_C}$, while $\frac{(1-\eta_C)\gamma_C}{\mu_C(\mu_C+\gamma_C+d_C)}$ accounts for infectiousness in carriers, weighted by reduced infectivity (η_C is immunity efficacy).
- Similarly, $\frac{p\delta_B\beta_{BT}\Pi_B}{\mu_B}\left(\frac{1}{\mu_B+\gamma_B+d_B} + \frac{(1-\eta_B)\gamma_B}{\mu_B(\mu_B+\gamma_B+d_B)}\right)$ estimates the number of ticks infected by a single infectious buffalo. These parameters mirror those for cattle but typically involve longer carrier durations, lower disease-induced mortality, and higher ecological exposure.
- It is important to note that the transmission of vector-borne diseases involves two sequential steps: from host to vector and from vector back to host. This two-step process justifies the use of the square root in the expression, capturing the combined effect of both transmission pathways on disease propagation.

2.3. Global stability analysis of the disease-free equilibrium

Our goal in this section is to establish the global stability of the DFE, following the approach outlined in Castillo-Chavez [22]. Let $X = (S_C, S_B, A_S) \in \mathbb{R}^3_+$ denote the uninfected populations, and $Y = (I_C, R_C, I_B, R_B, A_I) \in \mathbb{R}^5_+$ represent the infected populations. The model (2.5) can thus be expressed as:

$$X'(t) = F(X, Y),$$
$$Y'(t) = G(X, Y), \quad \text{with} \quad G(X, \mathbf{0}) = 0.$$

According to Castillo-Chavez [22], the DFE is globally asymptotically stable if the following conditions hold:

H1: For $X'(t) = F(X, \mathbf{0}) \geq 0$, the equilibrium is globally asymptotically stable.

Table 2
Number of possible positive roots of $g(A_I^\star)$ for $\mathcal{R}_0 < 1$ and $\mathcal{R}_0 > 1$.

Case	$\mathcal{Q}_0$	$\mathcal{Q}_1$	$\mathcal{Q}_2$	$\mathcal{R}_0$	Sign changes	Possible positive roots
1	+	+	+	$\mathcal{R}_0 < 1$	0	0
2	+	+	−	$\mathcal{R}_0 > 1$	1	1
3	+	−	+	$\mathcal{R}_0 < 1$	2	2
4	+	−	−	$\mathcal{R}_0 > 1$	1	1

H2: $G(X,Y) = UY - \tilde{G}(X,Y)$, where $\tilde{G}(X,Y) \geq 0$.

Here, $U = \mathcal{F} - \mathcal{V}$, with $\mathcal{F}$ and $\mathcal{V}$ defined in (2.7). For condition (H1), we have:

$$F(X,\mathbf{0}) = \begin{bmatrix} \Pi_C - \mu_C S_C \\ \Pi_B - \mu_B S_B \\ \Pi_T - \mu_A A_S \end{bmatrix}.$$

For condition (H2), it can be verified that:

$$\tilde{G}(X,Y) = \begin{bmatrix} (1-p)\beta_{TC} A_I \left(\frac{\Pi_C}{\mu_C} - S_C\right) \\ p\beta_{TB} A_I \left(\frac{\Pi_B}{\mu_B} - S_B\right) \\ (1-p)\beta_{CT}(I_C + (1-\eta_C)R_C)\left(\frac{\Pi_T}{\mu_T} - A_S\right) \\ +p\beta_{BT}(I_B + (1-\eta_B)R_B)\left(\frac{\Pi_T}{\mu_T} - A_S\right) \end{bmatrix}.$$

Therefore, whenever $\mathcal{R}_0 < 1$, the disease-free equilibrium (DFE) $\mathcal{E}^0$ is globally asymptotically stable. This implies that the DFE and the endemic equilibrium cannot coexist in the model (2.5). We claim the following result:

Theorem 2.1. *If $\mathcal{R}_0 < 1$, then the DFE $\mathcal{E}^0$ of model (2.5) is globally asymptotically stable.*

2.4. Existence and local stability of the endemic equilibrium

Let $\mathcal{E}^* = (S_C^\star, I_C^\star, R_C^\star, S_B^\star, I_B^\star, R_B^\star, A_S^\star, A_I^\star)$ be the endemic equilibrium of model (2.5). To determine its existence, we set the right-hand sides of the model equations to zero and solve all variables in terms of $A_I^\star$. This yields:

$$\begin{aligned}
S_C^\star &= \frac{\Pi_C}{(1-p)\delta_C\beta_{TC}A_I^\star + \mu_C}, \quad I_C^\star = \frac{(1-p)\delta_C\beta_{TC}A_I^\star\Pi_C}{a_1((1-p)\delta_C\beta_{TC}A_I^\star + \mu_C)}, \quad R_C^\star = \frac{\gamma_C(1-p)\delta_C\beta_{TC}A_I^\star\Pi_C}{a_1\mu_C((1-p)\delta_C\beta_{TC}A_I^\star + \mu_C)}, \\
S_B^\star &= \frac{\Pi_B}{p\delta_B\beta_{TB}A_I^\star + \mu_B}, \quad I_B^\star = \frac{p\delta_B\beta_{TB}A_I^\star\Pi_B}{a_2(p\delta_B\beta_{TB}A_I^\star + \mu_B)}, \quad R_B^\star = \frac{\gamma_B p\delta_B\beta_{TB}A_I^\star\Pi_B}{a_2\mu_B(p\delta_B\beta_{TB}A_I^\star + \mu_B)}, \\
A_S^\star &= \frac{\Pi_T a_1 a_2 (A_I^\star K_B + \mu_A)(A_I^\star K_B + \mu_A)}{a_1 k_B^2 K_C \Pi_B \alpha_B A_I^{\star 2} + a_2 K_B K_C \Pi_C \alpha_C A_I^{\star 2} + a_1 a_2 K_B K_C \mu_A A_I^{\star 2} + a_2 K_C^2 \Pi_C \alpha_C \mu_B A_I^\star + Z_1},
\end{aligned} \tag{2.9}$$

where

$$\begin{aligned}
&a_1 = \mu_C + \gamma_C + d_C, \quad a_2 = \mu_B + \gamma_B + d_B, \quad K_C = (1-p)\delta_C\beta_{CT}, \\
&K_B = p\delta_B\beta_{BT}, \quad \alpha_C = 1 + \frac{(1-\eta_C)\gamma_C}{\mu_C}, \quad \alpha_B = 1 + \frac{(1-\eta_B)\gamma_B}{\mu_B}, \\
&Z_1 = a_1 a_2 K_C \mu_A \mu_B A_I^\star + a_1 K_B^2 + \Pi_B \alpha_B \mu_C A_I^\star + a_1 a_2 K_B \mu_A \mu_C A_I^\star + a_1 a_2 \mu_C \mu_B \mu_A.
\end{aligned}$$

Substituting (2.9) into the last equation of model (2.5) yields a quadratic in $A_I^\star$:

$$g(A_I^\star) = \mathcal{Q}_0 A_I^{\star 2} + \mathcal{Q}_1 A_I^\star + \mathcal{Q}_2 = 0, \tag{2.10}$$

where

$$\begin{aligned}
\mathcal{Q}_0 &= a_1 a_2 K_C K_B \mu_A^2 + a_1 \alpha_B K_B K_C \mu_A + a_2 \alpha_C K_C K_B \mu_A, \\
\mathcal{Q}_1 &= \mu_A^2 a_1 a_2 (\mu_C K_B + \mu_B K_C) + \mu_A(\alpha_C K_C a_2 \mu_B + \alpha_B K_B a_1 \mu_C) - \mu_A^2 a_1 a_2 \mu_C \mu_B \mathcal{R}_0^2, \\
\mathcal{Q}_2 &= \mu_A^2 a_1 a_2 \mu_C \mu_B (1 - \mathcal{R}_0^2).
\end{aligned}$$

Since all parameters and variables are nonnegative, we apply Descartes' Rule of Signs to determine the number of positive roots of (2.10) for $\mathcal{R}_0 < 1$ and $\mathcal{R}_0 > 1$. Notably, $\mathcal{R}_0 = 1$ is the bifurcation point. The sign analysis summarized in Table 2.

Based on these cases, the following results are established:

Theorem 2.2. *The model (2.5) admits:*

(i) a unique endemic equilibrium $\mathcal{E}^*$ if $\mathcal{R}_0 > 1$ and cases 2 or 4 occur,
(ii) multiple endemic equilibria if $\mathcal{R}_0 < 1$ and case 3 holds,
(iii) no endemic equilibrium if $\mathcal{R}_0 < 1$ and cases 1 or part of case 3 are satisfied.

To analyze the local stability of $\mathcal{E}^*$, we employ the Center Manifold Theorem (CMT) as presented in Castillo-Chavez [23]. Extensive calculations, detailed in Appendix A, lead to the following key result:

Theorem 2.3. *Model (2.5) exhibits a forward bifurcation at the critical threshold $\mathcal{R}_0 = 1$.*

This indicates that as $\mathcal{R}_0$ passes through 1, the system transitions from a disease-free state to an endemic equilibrium, signifying a bifurcation.

2.5. Formulation of the optimal control problem

In this section, we employ optimal control theory to assess the impact of combining multiple intervention strategies aimed at minimizing the number of infected cattle over time while incurring minimal costs. Specifically, we examine how integrating optimized acaricide use, cattle vaccination, and habitat modification can reduce infection prevalence. Optimal control analysis is a powerful mathematical tool for managing and mitigating epidemic diseases by identifying the most efficient intervention strategies. The results provide actionable insights for policymakers, enabling targeted and cost-effective implementation. For example, the analysis may suggest that a combination of widespread vaccination and acaricide application is the most effective approach to controlling disease spread. These strategies are commonly employed mechanisms for managing tick-borne infections. Let $u_1(t)$, $u_2(t)$, and $u_3(t)$ denote the control functions corresponding to acaricide application, vaccination, and habitat modification, respectively. We formulate the following objective functional to be minimized:

$$J(u_1(t), u_2(t), u_3(t)) = \int_0^T \left[A_1 I_C(t) + A_2 R_C(t) + A_3 N_T + \frac{1}{2} w_1 u_1^2(t) + \frac{1}{2} w_2 u_2^2(t) + \frac{1}{2} w_3 u_3^2(t)\right] dt, \tag{2.11}$$

subject to the constraints:

$$\begin{aligned}
S_C'(t) &= \Pi_C - (1-u_1(t))\lambda_{TC} S_C - \mu_C S_C - u_2(t) S_C,\\
I_C'(t) &= (1-u_1(t))\lambda_{TC} S_C - (\mu_C + \gamma_C + d_C) I_C,\\
R_C'(t) &= u_2(t) S_C + \gamma_C I_C - \mu_C R_C,\\
S_B'(t) &= \Pi_B - \lambda_{TB} S_B - \mu_B S_B,\\
I_B'(t) &= \lambda_{TB} S_B - (\mu_B + \gamma_B + d_B) I_B,\\
R_B'(t) &= \gamma_B I_B - \mu_B R_B,\\
A_S'(t) &= \Pi_T - (1-u_1(t))\lambda_{CT} A_S - \lambda_{BT} A_S - (\mu_A + u_3(t)) A_S,\\
A_I'(t) &= (1-u_1(t))\lambda_{CT} A_S + \lambda_{BT} A_S - (\mu_A + u_3(t)) A_I,
\end{aligned} \tag{2.12}$$

In the objective functional (2.11), the positive constants A_1, A_2, A_3, w_1, w_2, and w_3 weight the importance of infected cattle, recovered cattle, total tick population, and the costs associated with each control. This formulation effectively translates the integral into monetary expenditure over a finite period T. The choice of quadratic controls is motivated by their mathematical advantages: (i) they simplify the process of finding optimal solutions, and (ii) they are smooth functions with a single extremum [24].

The optimal control problem involves determining control functions $U = (u_1^*(t), u_2^*(t), u_3^*(t))$ that minimize J:

$$J(u_1^*(t), u_2^*(t), u_3^*(t)) = \inf_{(u_1,u_2,u_3)\in U} J(u_1(t), u_2(t), u_3(t)), \tag{2.13}$$

where the admissible set U is defined as:

$$U = \left\{(u_1(t), u_2(t), u_3(t)) \in (L^\infty(0, t_f))^3 \,:\, 0 \le u_i(t) \le u_{i\max}, \quad i = 1, 2, 3\right\},$$

and $u_{i\max}$ are positive bounds on the control functions.

The optimal controls are obtained by solving the necessary conditions derived via Pontryagin's Maximum Principle (PMP) [25] or alternative methods such as dynamic programming [26]. In this work, we apply PMP and define the Hamiltonian:

$$\begin{aligned}
\mathcal{H}(t, \mathbf{x}, \mathbf{u}, \lambda) &= A_1 I_C(t) + A_2 R_C(t) + A_3 N_T + \frac{1}{2} w_1 u_1^2(t) + \frac{1}{2} w_2 u_2^2(t) + \frac{1}{2} w_3 u_3^2(t)\\
&\quad + \sum_{k=1}^{8} \lambda_k f_k,
\end{aligned} \tag{2.14}$$

where $\lambda = [\lambda_1(t), \lambda_2(t), \ldots, \lambda_8(t)]$ are the adjoint variables associated with the 8-dimensional state vector $\mathbf{x} = (S_C, I_C, R_C, S_B, I_B, R_B, A_S, A_I)$, and f_k corresponds to the right-hand side of the kth state equation in (2.12) with $k = 1, \ldots, 8$. The necessary conditions for optimality are detailed in Appendix B.

Table 3
Cumulative monthly cases from December 2014 to December 2020.

Year	Months											
	Jan	Feb	Mar	Apr	May	Jun	Jul	Aug	Sept	Oct	Nov	Dec
2014												178
2015	179	180	183	187	192	198	204	212	220	229	238	243
2016	266	299	343	395	452	511	569	624	671	709	734	743
2017	735	712	678	636	587	536	485	436	394	360	337	329
2018	340	372	423	490	572	667	771	885	1005	1129	1255	1381
2019	1531	1724	1952	2204	2472	2747	3020	3283	3525	3739	3914	4043
2020	4145	4244	4340	4431	4517	4595	4664	4724	4773	4809	4832	4840

3. Numerical results and discussions

In this section, we employ several numerical techniques to solve the basic model (2.5) and the optimal control problem (2.12). We first present results for the basic model, offering insights into its behavior and dynamics. Next, we analyze the optimal control problem, illustrating how the optimal strategies influence system evolution and target outcomes.

3.1. Parameter estimation and model fitting

Parameter estimation and model fitting are essential in epidemiological modeling. They support model validation, calibration, and enable future predictions [27]. Additionally, these processes provide valuable insights into the transmission dynamics of the disease under investigation, enhancing our understanding of the underlying mechanisms [28]. In this study, some model parameters were adopted from previously published peer-reviewed articles, ensuring biological plausibility and consistency with existing literature. Other parameters were determined through a systematic fitting process to observed data. To perform the fitting, we employed the least-squares estimation technique, which minimizes discrepancies between observed and model-predicted data. Specifically, the cumulative monthly reported cases of ECF in Zimbabwe, obtained from a report by the Department of Veterinary Services covering December 2014 to December 2020, served as the data source [29] (see Table 3). The parameter estimation procedure utilized MATLAB's optimization routine *fmincon* to minimize an objective function subject to specified bounds for the parameters [28]. The objective function was defined as the sum of squared residuals between the observed monthly incidence data and the model's predictions. Mathematically, this optimization problem can be expressed as:

$$\min_{\theta} \sum_{i=1}^{n} \left(I_{obs}(t_i) - I_{model}(t_i, \theta) \right)^2, \tag{3.1}$$

where $I_{obs}(t_i)$ denotes the observed incidence at time t_i, $I_{model}(t_i, \theta)$ is the model-predicted incidence, and θ is the vector of unknown parameters and initial conditions [28]. During the optimization, the system of ODEs was numerically solved using the fourth-order Runge–Kutta (RK4) method with monthly steps ($\Delta t = 1$). The primary goal was to minimize the sum of squared differences between data points and model outputs, ensuring an accurate fit [30]. All baseline parameters obtained from this fitting process are presented in Table 5. The initial conditions were assumed as follows: $N_C = 85,000$, $N_B = 75,000$, $N_T = 100,000$, $I_C(0) = 171$, $R_C(0) = 1$, $I_B(0) = 7500$, $R_B(0) = 0$, and $A_I(0) = 9944$.

Fig. 2 illustrates the quality of the model fit, demonstrating that the model aligns well with the observed data. Based on this fit, the model can be confidently used for future predictions regarding the dynamics of ECF in cattle, buffaloes, and ticks. During the fitting process, key parameters such as transmission rates (β_{TC}, β_{CT}, β_{TB}, β_{BT}), host recruitment rates (Π_C, Π_B), and vector recruitment rate (Π_T) were directly estimated from data. Parameters including recovery rates (γ_C, γ_B), attachment rates (δ_C, δ_B), natural mortality (μ_C, μ_B), disease-induced death rates (d_C, d_B), and transmission efficiencies (η_C, η_B) were obtained from literature (see Tables 4 and 5). Uncertainty in parameter estimates was quantified using the delta method to derive 95% confidence intervals [28]. As expected, these intervals are relatively broad, reflecting uncertainty due to data limitations.

Fig. 2 indicates that ECF cases remained relatively low and stable between 2014 and 2015, with a moderate increase in 2015–2016, a slight decline around 2017, and a sharp rise from 2017 onward. Both observed data and model predictions show rapid epidemic growth in 2018–2019. By 2020, cases approached approximately 5000. The model effectively captures the overall trend, especially the exponential increase post-2017. Minor discrepancies during 2016–2017 reflect short-term fluctuations, but the general agreement remains satisfactory. The widening confidence intervals over time reflect increasing uncertainty as the epidemic progresses. Parameter estimates are biologically plausible and align with existing literature on tick-host-pathogen dynamics. The final estimates and confidence intervals are summarized in Table 4.

3.2. Sensitivity analysis of the reproduction number

As previously highlighted, $\mathcal{R}_0$ is a critical metric in infectious disease modeling. It is essential to identify the parameters that most strongly influence its value. To this end, we compute the normalized forward sensitivity indices, which quantify the relative

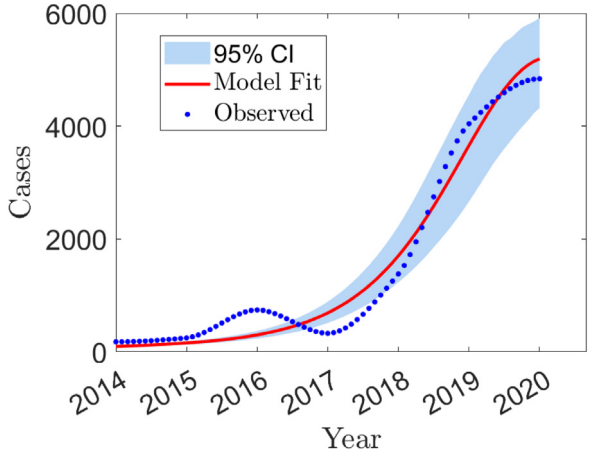

Fig. 2. Observed ECF cases and the fitted model over 2014–2020. Blue dots show cumulative cases; the red curve indicates the model fit; light-blue shading represents the 95% confidence interval.

Table 4
Fitted parameter values and 95% confidence intervals.

Parameter	Estimate (Mean)	95% CI Lower	95% CI Upper
Π_C	3.56073×10^{3}	3.21731×10^{3}	3.89936×10^{3}
Π_B	9.18942×10^{2}	8.31486×10^{2}	1.00767×10^{3}
Π_T	4.37366×10^{3}	3.96292×10^{3}	4.78963×10^{3}
β_{TC}	3.08073×10^{-7}	2.78403×10^{-7}	3.37672×10^{-7}
β_{CT}	9.99968×10^{-7}	9.05586×10^{-7}	1.09340×10^{-6}
β_{TB}	9.95227×10^{-7}	9.01412×10^{-7}	1.08859×10^{-6}
β_{BT}	2.83286×10^{-11}	2.56579×10^{-11}	3.10555×10^{-11}

Table 5
Parameters from literature.

Symbol	Definition	Value	Units	Source
β_{TC}	Tick to cattle transmission	3.08073×10^{-7}	Month^{-1}	Fitting
β_{TB}	Tick to buffalo transmission	9.95227×10^{-7}	Month^{-1}	Fitting
β_{CT}	Cattle to tick transmission	9.99968×10^{-7}	Month^{-1}	Fitting
β_{BT}	Buffalo to tick transmission	2.83286×10^{-11}	Month^{-1}	Fitting
p	Proportion of tick bites on buffalo	0.20	Dimensionless	Fitting
Π_C	Cattle recruitment rate	3.56073×10^{3}	Month^{-1}	Fitting
Π_B	Buffalo recruitment rate	9.18942×10^{2}	Month^{-1}	Fitting
Π_T	Tick recruitment rate	4.37366×10^{3}	Month^{-1}	Fitting
η_C, η_B	Transmission efficiency (carriers)	0.99	Dimensionless	[3]
μ_A	Tick mortality rate	1.9841×10^{-4}	Month^{-1}	[3]
δ_C	Attachment rate on cattle	0.77	Dimensionless	[3]
δ_B	Attachment rate on buffalo	0.77	Dimensionless	[3]
μ_C	Natural mortality (cattle)	2.44085×10^{-5}	Month^{-1}	[3]
μ_B	Natural mortality (buffalo)	1.4269×10^{-5}	Month^{-1}	[3]
γ_C	Recovery rate (cattle)	5.5556×10^{-3}	Month^{-1}	[3]
γ_B	Recovery rate (buffalo)	5.5556×10^{-3}	Month^{-1}	[3]
d_C	ECF death rate (cattle)	7.9365×10^{-3}	Month^{-1}	[3]
d_B	ECF death rate (buffalo)	2.3148×10^{-4}	Month^{-1}	[3]

impact of each parameter on $\mathcal{R}_0$. Parameters with negative sensitivity indices imply that increasing these parameters decreases $\mathcal{R}_0$, while those with positive indices suggest that their increase elevates $\mathcal{R}_0$. The sensitivity index, denoted as $\zeta_P^{\mathcal{R}_0}$, is defined as:

$$\zeta_P^{\mathcal{R}_0} = \frac{P}{\mathcal{R}_0} \times \frac{\partial \mathcal{R}_0}{\partial p}. \tag{3.2}$$

Using the baseline parameter values listed in Table 5, we calculated the sensitivity indices shown in Fig. 3. The results indicate that parameters such as Π_C, β_{TC}, β_{CT}, δ_C, γ_C, Π_B, β_{TB}, β_{BT}, δ_B, γ_B, and Π_T have positive sensitivities. This means that proportional increases in these parameters will raise $\mathcal{R}_0$, thereby enhancing the potential for disease transmission and spread. Conversely, parameters like η_C, μ_A, d_C, μ_C, μ_B, d_B, and η_B exhibit negative sensitivities—meaning that increasing these parameters will decrease $\mathcal{R}_0$. These findings highlight key parameters that could be targeted in control strategies to effectively reduce disease transmission.

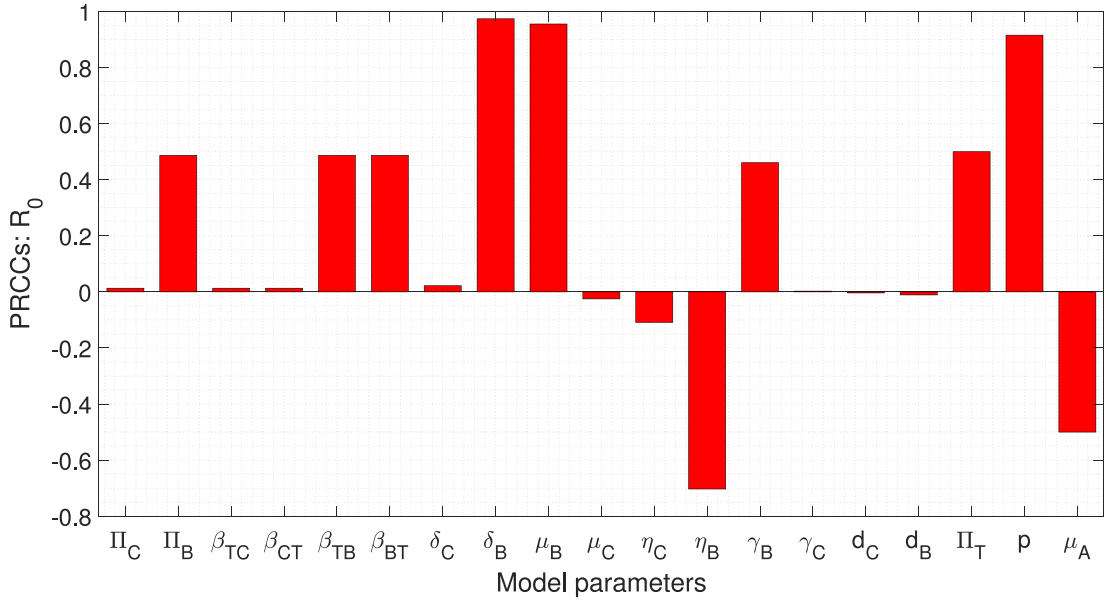

Fig. 3. Sensitivity analysis illustrating the relationship between $\mathcal{R}_0$ and model parameters.

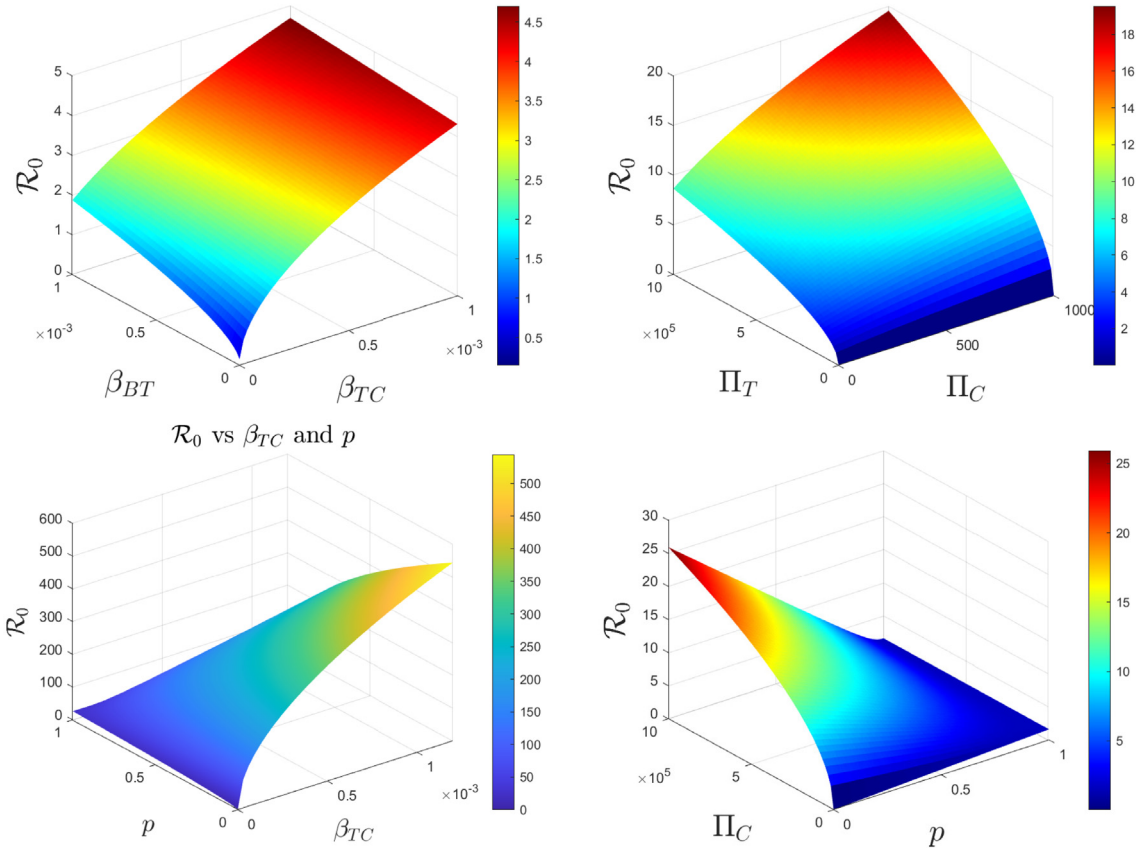

Fig. 4. Surface plots illustrating the relationship between $\mathcal{R}_0$ and two model parameters.

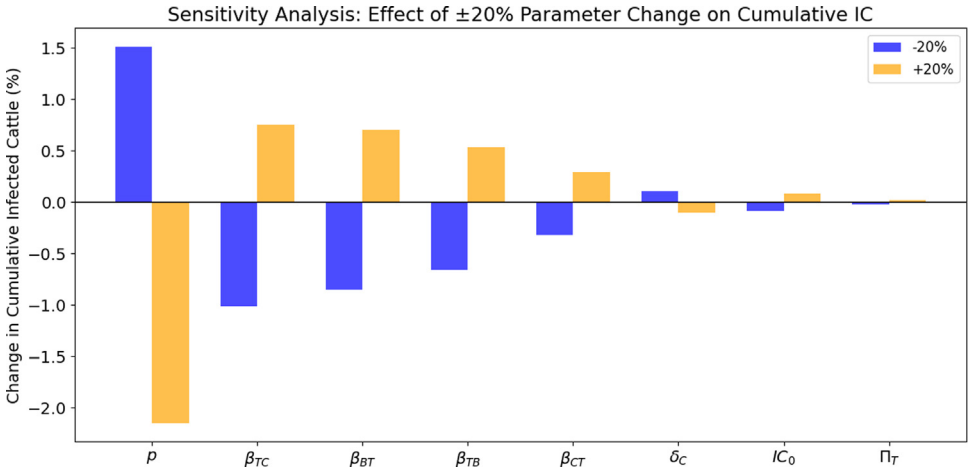

Fig. 5. Sensitivity analysis: Effect of ±20% variation in parameters on the peak number of infected cattle. Bars indicate the change in peak infected cattle (I_C) following a 20% increase (orange) or decrease (blue) in each parameter. Only parameters with significant influence are shown.

The sensitivity analysis in Fig. 3 was conducted by varying one parameter at a time while holding others constant. To explore the combined effects of two transmission-related parameters, we simulated $\mathcal{R}_0$ as a function of these parameters. The results, depicted in Fig. 4, are consistent with the local sensitivity analysis. Specifically, increasing two parameters positively correlated with $\mathcal{R}_0$ — such as the transmission rates — significantly elevates its value. For instance, in Fig. 4(a), increasing both the tick-to-cattle transmission rate β_{TC} and the cattle-to-tick transmission rate β_{CT} markedly raises $\mathcal{R}_0$. Conversely, increasing two parameters negatively correlated with $\mathcal{R}_0$ results in a substantial decrease. It is important to note that since $\mathcal{R}_0$ incorporates parameters associated with disease transmission within wildlife populations, an increase in these transmission rates also elevates $\mathcal{R}_0$. This underscores the potential risk of spillover from wildlife reservoirs to livestock, highlighting the importance of controlling wildlife transmission to mitigate outbreaks in cattle and buffalo.

3.3. Global sensitivity analysis

To identify the key factors influencing disease dynamics, we conducted a comprehensive global sensitivity analysis using Latin Hypercube Sampling (LHS) combined with the Partial Rank Correlation Coefficients (PRCC) method, as outlined in Marino et al. [31]. The results are presented in Fig. 5. The results reveal that the proportion of tick bites on buffalo (p) has the greatest impact on the cumulative infected cattle. This is followed by the tick-to-cattle transmission rate (β_{TC}), the buffalo-to-tick transmission rate (β_{BT}), and the cattle-to-tick transmission rate (β_{CT}). Moderate effects are observed for the tick-to-buffalo transmission rate (β_{TB}) and the initial infected cattle population ($I_C(0)$). Parameters such as the tick recruitment rate (Π_T) and the immune cattle infection modifier (δ_C) exhibit minimal influence. Notably, the negative correlation associated with increasing p underscores the key role of tick feeding preferences in shaping the long-term infection burden in cattle. These findings suggest that targeted interventions — such as reducing tick feeding on buffalo hosts or modifying transmission pathways — could significantly decrease infection prevalence in cattle populations.

3.4. Predicting future disease dynamics

To evaluate the long-term impact of East Coast Fever (ECF) in Zimbabwe, we projected the model from 2021 to 2030. These simulations assume no changes in control measures or environmental conditions beyond 2020 (see Fig. 6). This baseline scenario isolates the intrinsic disease dynamics under current practices, a common approach in epidemiological modeling that facilitates interpretation without speculative assumptions. The projection serves as a quantitative reference for understanding potential disease burden and guiding future control strategies. Fig. 6 illustrates that the model predicts a gradual decline in ECF cases over the projection period. From 2026 to 2030, cases are expected to be lower and stable. The model estimates that monthly cases will be approximately 2500. This indicates that the sharp growth observed during the 2014–2020 outbreak phase is unlikely to be sustained from 2026 to 2030. Instead, disease dynamics tend to approach a lower equilibrium, implying persistent but controlled transmission within the host-vector system. The widening confidence interval immediately after the forecast point reflects uncertainty in long-term predictions, while the subsequent narrowing suggests increasing confidence in the projected endemic trend. Overall, the model indicates a transition from epidemic growth to endemic stabilization after 2020, offering valuable insights for long-term surveillance, resource allocation, and strategic control planning.

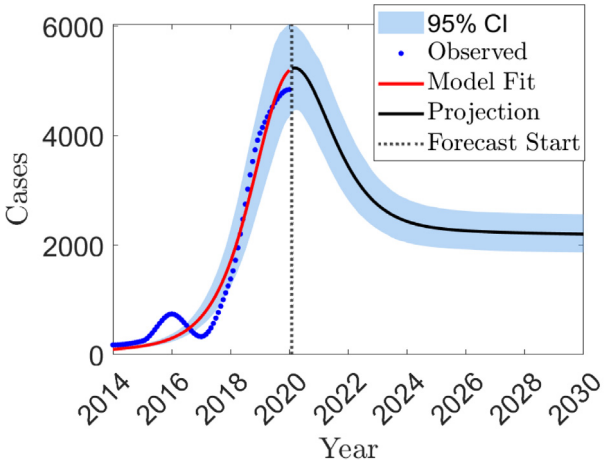

Fig. 6. The model-fitted (2014–2020) and projected dynamics of ECF cases from 2020 to 2030. Blue dots represent observed cases, the red curve shows the fitted model, the black curve indicates projected cases beyond 2020, and the shaded light-blue region denotes the 95% confidence interval (CI). The vertical dotted line marks the start of the forecast in 2020.

Table 6
Projected population levels as of June 2026.

Variable	Number of hosts
Susceptible cattle $S_C(t)$	2.77×10^4
Infectious cattle $I_C(t)$	2.84×10^5
Recovered cattle $R_C(t)$	1.25×10^5
Susceptible buffaloes $S_B(t)$	1.10×10^4
Infectious buffaloes $I_B(t)$	1.39×10^5
Recovered buffaloes $R_B(t)$	5.96×10^4
Susceptible ticks $A_S(t)$	2.48×10^4
Infectious ticks $A_I(t)$	7.14×10^5

3.5. Optimal control simulation results

In this section, we present the outcomes of various optimized control strategies under different scenarios. Specifically, we report numerical results for the optimal control problem (2.12), which was solved by addressing the associated optimality system—eight coupled ordinary differential equations derived from the state and costate equations. The widely used forward–backward sweep method [32] was employed for the numerical solution. Additionally, we assess the potential impact of rolling control strategies starting from July 2026. The initial population levels used are shown in Table 3; these were estimated using data from Table 6 and represent the expected populations by the end of June 2026.

The three intervention strategies considered are acaricide application, vaccination, and habitat modification, represented by control functions $u_1(t)$, $u_2(t)$, and $u_3(t)$, respectively. To account for feasibility constraints, each control was assigned an upper bound reflecting operational and ecological limitations: acaricide efficacy is capped at 70%–80%, vaccination coverage at 80%–85%, and habitat management at 80%–85%, due to supply constraints and heterogeneous uptake. For the weights in the objective functional, we set $A_1 = A_2 = A_3 = 5$, indicating equal emphasis on minimizing the number of infected cattle and carriers. Considering Zimbabwe's context and previous cost analyses [33], habitat modification is typically the most expensive intervention, followed by vaccination, with acaricide application being the least costly. To incorporate these cost considerations, we assigned weights such that $w_3 > w_2 > w_1$, specifically $w_3 = 20$, $w_2 = 10$, and $w_1 = 5$. This penalizes more costly interventions within the optimization process. It is worth noting that vaccination costs vary depending on the method used — such as dipping versus spraying — and regional factors; thus, these weights are based on assumptions and should be adjusted to reflect local economic conditions.

Our analysis considers the following strategies:

- **Strategy A**: Acaricide application only ($u_1 \neq 0$, $u_2 = 0$, $u_3 = 0$)
- **Strategy B**: Acaricide plus vaccination ($u_1 \neq 0$, $u_2 \neq 0$, $u_3 = 0$)
- **Strategy C**: Acaricide plus habitat modification ($u_1 \neq 0$, $u_2 = 0$, $u_3 \neq 0$)
- **Strategy D**: All three measures combined ($u_1 \neq 0$, $u_2 \neq 0$, $u_3 \neq 0$)

Each scenario provides insights into the effectiveness and cost-efficiency of different intervention combinations in reducing the infected cattle population.

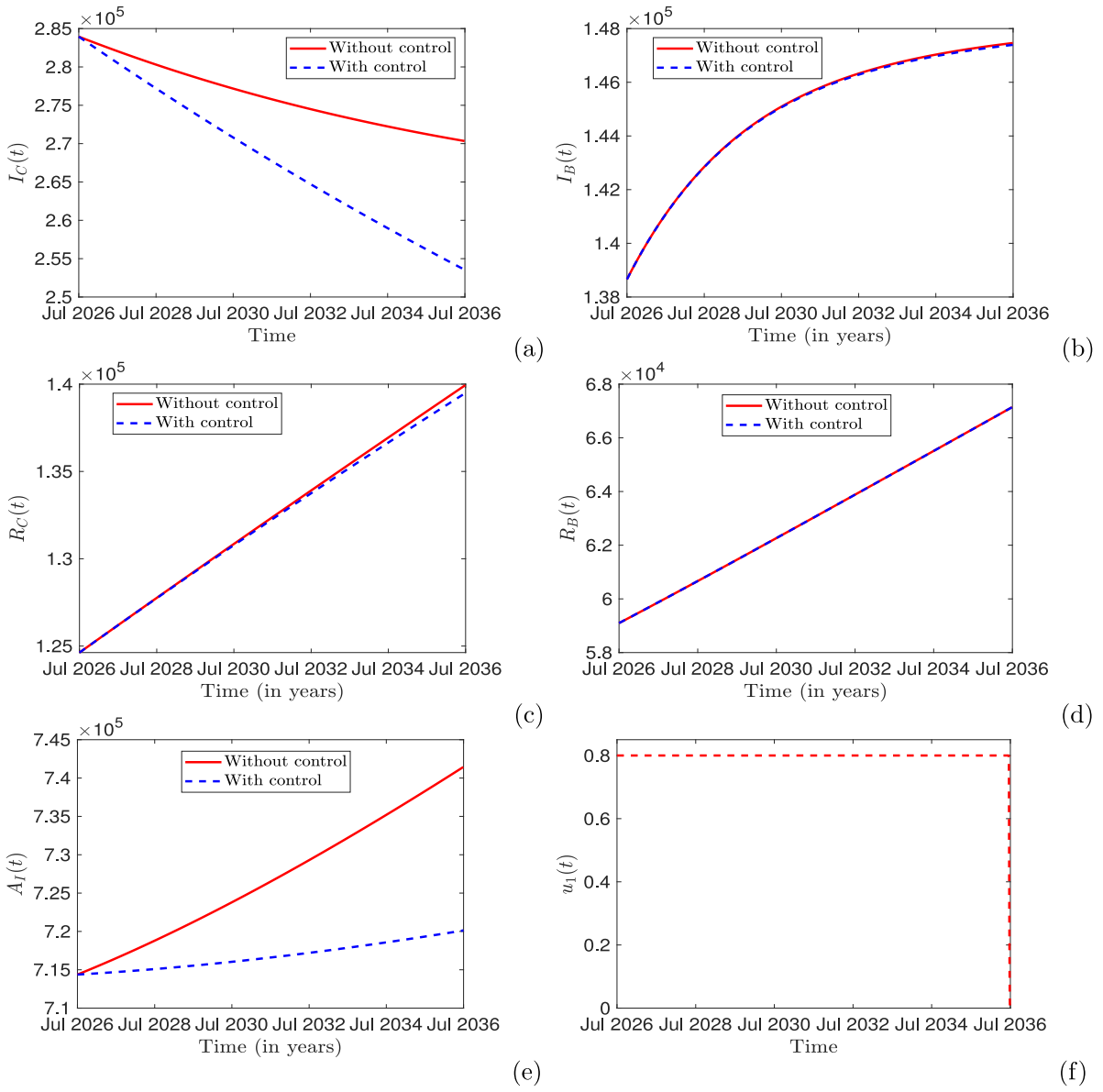

Fig. 7. Simulation results for Strategy A (Optimal acaricide application) with $0 \leq u_1(t) \leq 0.80$. The solid red curves represent population levels without control, while the dashed black curves depict populations under control measures. (a) Number of infectious cattle $I_C(t)$; (b) Number of infectious buffaloes $I_B(t)$; (c) Recovered cattle $R_C(t)$; (d) Recovered buffaloes $R_B(t)$; (e) Infectious ticks; (f) Time-varying optimal acaricide application rates.

Strategy A: Optimal acaricide use alone ($u_1 \neq 0, u_2 = 0, u_3 = 0$)

Application of acaricides through animal dipping is one of the most widely adopted strategies in Zimbabwe, primarily due to its relatively low cost and straightforward implementation. The primary objective of Strategy A is to evaluate the efficacy of acaricide use as the sole control measure. To this end, the control variables associated with vaccination and habitat modification are set to zero, while the acaricide application control $u_1(t)$ is allowed to vary within the range $[0, 0.8]$. The results are depicted in Fig. 7.

Results in Fig. 7(a) demonstrate that acaricide control significantly reduces the infectious cattle population $I_C(t)$ compared to the uncontrolled case. Under control, $I_C(t)$ declines more rapidly over time, indicating effective suppression of tick-mediated transmission and a decrease in disease prevalence among cattle. Fig. 7(b) shows the dynamics of the infectious buffalo population $I_B(t)$. Both controlled and uncontrolled trajectories exhibit gradual growth toward equilibrium; however, the controlled trajectory remains slightly lower, suggesting limited indirect effects of acaricide intervention on buffalo. Figs. 7(c) and (d) depict the recovered cattle $R_C(t)$ and recovered buffalo $R_B(t)$ populations, respectively. In both, trajectories are relatively close, indicating that acaricide application primarily targets disease transmission rather than significantly affecting long-term recovery dynamics. For the infectious

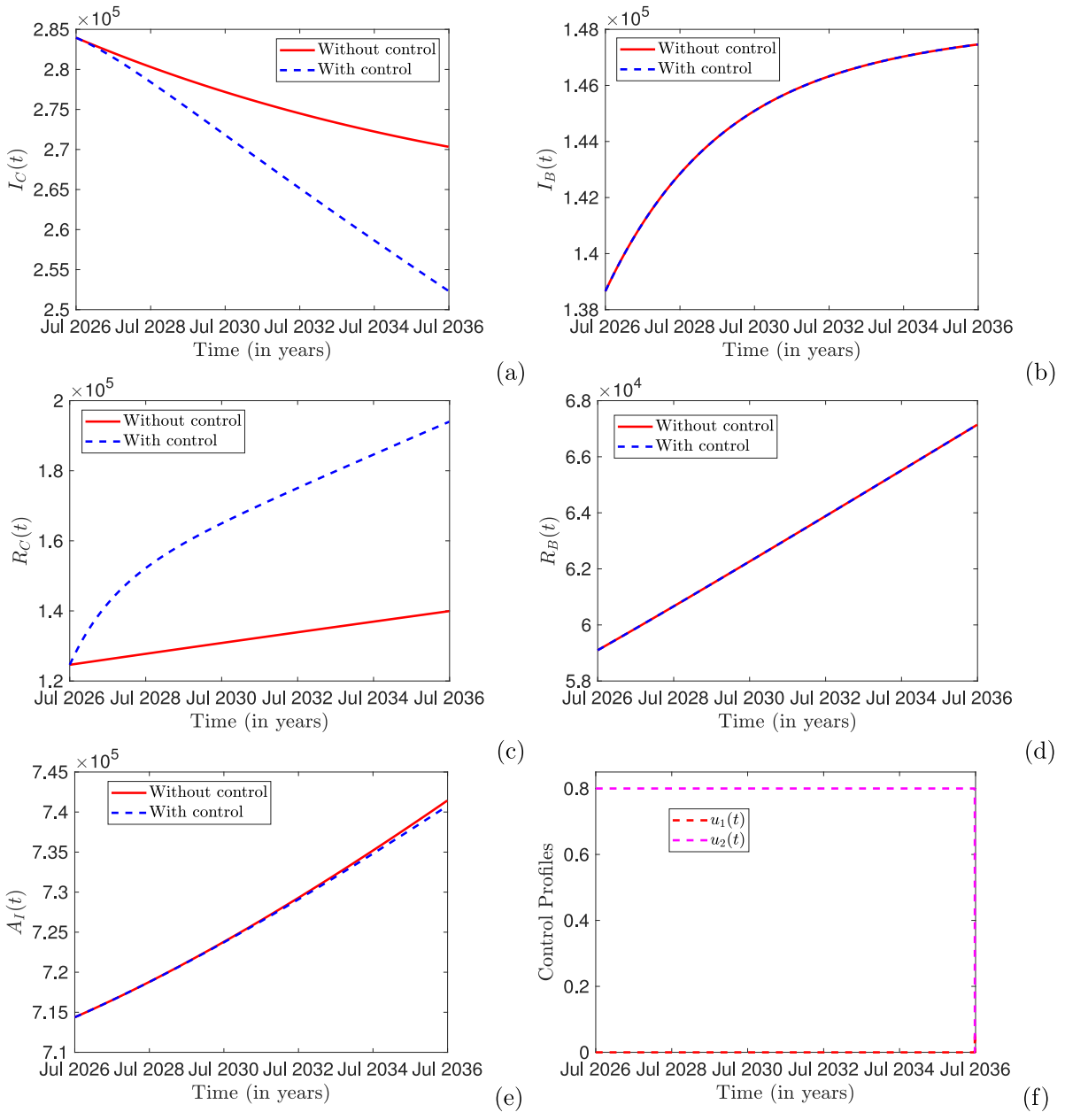

Fig. 8. Simulation results for Strategy B (optimal vaccination and acaricide application) with control bounds $0 \le u_1(t) \le 0.8$ and $0 < u_2(t) \le 0.60$. Solid red curves represent populations without control interventions, while dashed black curves depict populations under control strategies. Panels $(a)-(b)$ display infectious cattle and buffalo populations, respectively; panels $(c)-(d)$ show recovered cattle and buffalo populations; panel (e) depicts infectious ticks; and panel (f) illustrates the time-varying optimal control rates.

tick population $A_I(t)$ in Fig. 7(e), the uncontrolled scenario shows a continuous increase in tick abundance, whereas the controlled trajectory remains substantially lower throughout the simulation. This confirms that optimal acaricide application effectively suppresses infectious ticks, interrupting pathogen transmission between hosts. Fig. 7(f) illustrates the optimal control profile $u_1(t)$, which remains at a high level throughout the 10-year intervention. This suggests that sustained, intensive acaricide application is necessary to achieve significant reductions in infectious ticks and ECF prevalence in hosts.

In summary, Strategy A (optimal acaricide use) effectively reduces infectious cattle and limits tick population growth. However, its impact on buffalo-related compartments is minimal. These findings indicate that, although optimizing acaricide application markedly decreases new infections when used alone, it may not suffice for complete disease eradication. This highlights the importance of integrating additional control strategies to enhance overall disease management.

Strategy B: Optimal acaricide use combined with vaccination ($u_1 \neq 0, u_2 \neq 0, u_3 = 0$)

In this strategy (Strategy B), we analyze the impact of optimizing acaricide application and cattle vaccination to mitigate the spread of East Coast Fever (ECF). The results are illustrated in Fig. 8. The results in Fig. 8(a) show that the combined optimal control strategy — comprising acaricide application $u_1(t)$ and vaccination $u_2(t)$ — produces a substantial reduction in the infectious cattle population $I_C(t)$ over the simulation horizon. Under control, $I_C(t)$ declines more rapidly than in the uncontrolled scenario, decreasing from approximately 2.84×10^5 to nearly 2.52×10^5 by July 2036. In contrast, the uncontrolled trajectory shows only minimal decline. This demonstrates that integrating acaricide and vaccination effectively suppresses disease transmission and reduces infection burden within cattle. Fig. 8(b) indicates that the infectious buffalo population $I_B(t)$ increases gradually in both scenarios, with the controlled trajectory remaining marginally lower throughout the simulation. A notable improvement is observed in the recovered (carrier) cattle population $R_C(t)$ (Fig. 8(c)). The controlled system yields a substantially larger recovered population — approximately 1.93×10^5 — compared to the uncontrolled case, reflecting enhanced immunity acquisition and survival due to vaccination. By the end of the intervention, the recovered class under control exceeds the uncontrolled trajectory, underscoring vaccination's role in increasing recovery and long-term herd immunity.

In Fig. 8(d), both controlled and uncontrolled trajectories are nearly identical, indicating minimal direct impact on buffalo dynamics. This aligns with the fact that the intervention primarily targeted cattle via vaccination and ticks via acaricide application, without explicit buffalo-focused measures. Similarly, the tick population $A_I(t)$ shown in Fig. 8(e) exhibits only slight differences between scenarios. Although acaricide application contributed to some suppression of infected ticks, the reduction was modest over the long-term simulation, suggesting that additional vector-targeted strategies or increased acaricide coverage may be necessary to achieve stronger tick reductions. The optimal control profiles in Fig. 8(f) reveal that vaccination $u_2(t)$ was maintained at a consistently high level throughout most of the intervention period, while acaricide application $u_1(t)$ remained comparatively low. This indicates that vaccination was the dominant intervention for minimizing disease prevalence and optimizing the objective functional.

Overall, the combined acaricide–vaccination strategy demonstrated significant epidemiological benefits, notably in reducing infectious cattle and enhancing recovery. The results suggest that vaccination plays a central role in disease mitigation, with acaricide application providing supportive vector suppression. Consequently, integrating both measures offers a more effective approach to controlling ECF transmission compared to single interventions alone.

Strategy C: Optimal acaricide use combined with habitat modification (pasture management) ($u_1 \neq 0, u_3 \neq 0, u_2 = 0$)

Due to the high costs and limited availability of vaccines, vaccination is rarely employed as a control measure for East Coast Fever (ECF) in Zimbabwe. Conversely, farmers often adopt low-cost habitat modification techniques, such as controlled or prescribed burns, to manage tick populations. These burns are carefully planned and executed to reduce ground vegetation, leaf litter, and other tick habitats, thereby effectively decreasing tick densities. In this section, we evaluate the impact of combining acaricide application with habitat management on ECF transmission. The results are shown in Fig. 9. Fig. 9(a) illustrates the dynamics of the infectious cattle population $I_C(t)$. Under the control scenario, $I_C(t)$ declines markedly from approximately 2.84×10^5 to nearly 2.48×10^5 by July 2036, while the uncontrolled trajectory shows only a gradual decrease. This significant reduction demonstrates that combining acaricide use with habitat modification effectively suppresses transmission by targeting infected ticks and reducing environmental conditions favorable to tick survival. Fig. 9(b) shows the infectious buffalo population $I_B(t)$. Initially, it increases slightly in both scenarios but then declines steadily under control, reaching nearly 1.35×10^5. This suggests that the combined strategy can reduce disease prevalence in buffalo populations over time.

The recovered cattle population $R_C(t)$, depicted in Fig. 9(c), increases gradually in both cases, with only minor differences. Although the intervention reduces transmission and exposure, the small increase in recovered animals indicates that this strategy mainly prevents new infections rather than significantly enhancing recovery after infection. Similarly, Fig. 9(d) shows that buffalo recovered populations follow a comparable trend, with minimal differences, which is expected since the control primarily targets vectors and environmental conditions rather than buffalo directly. Fig. 9(e) displays the infected tick population $A_I(t)$. Notably, under the control scenario, the infected tick population declines sharply from about 7×10^5 to near elimination within a few years. In contrast, the uncontrolled tick population remains persistently high. This dramatic decline confirms that combining acaricide application with habitat modification disrupts tick survival, reproduction, and persistence, thus reducing disease transmission. The optimal control profiles in Fig. 9(f) show that both acaricide application $u_1(t)$ and habitat modification $u_3(t)$ are maintained at high levels during most of the intervention period, then decline sharply near the end. This pattern indicates that sustained application of both controls is necessary to achieve significant reductions in tick populations and disease spread. The simultaneous high application underscores the synergistic effect of vector-targeted and environmental interventions.

Overall, the combined acaricide–habitat modification strategy demonstrates strong epidemiological effectiveness, particularly in reducing infected tick populations and infection among cattle and buffalo. These results suggest that integrating direct vector control with environmental management can substantially disrupt disease transmission pathways and serve as a highly effective long-term approach for controlling ECF in endemic regions.

Strategy D: Implementation of all three control measures simultaneously ($u_1 \neq 0$, $u_2 \neq 0$, $u_3 \neq 0$)

In this section, we evaluate the effects of simultaneously optimizing all three intervention strategies on disease mitigation. The results are shown in Fig. 10. Fig. 10(a) depicts the dynamics of the infectious cattle population $I_C(t)$. Under the uncontrolled scenario, $I_C(t)$ declines gradually over time. In contrast, the controlled trajectory exhibits a much steeper decline, decreasing from approximately 2.84×10^5 to nearly 2.48×10^5 by July 2036. This reduction indicates that integrated implementation of acaricide use, vaccination, and habitat modification effectively interrupts transmission pathways and suppresses infection progression within

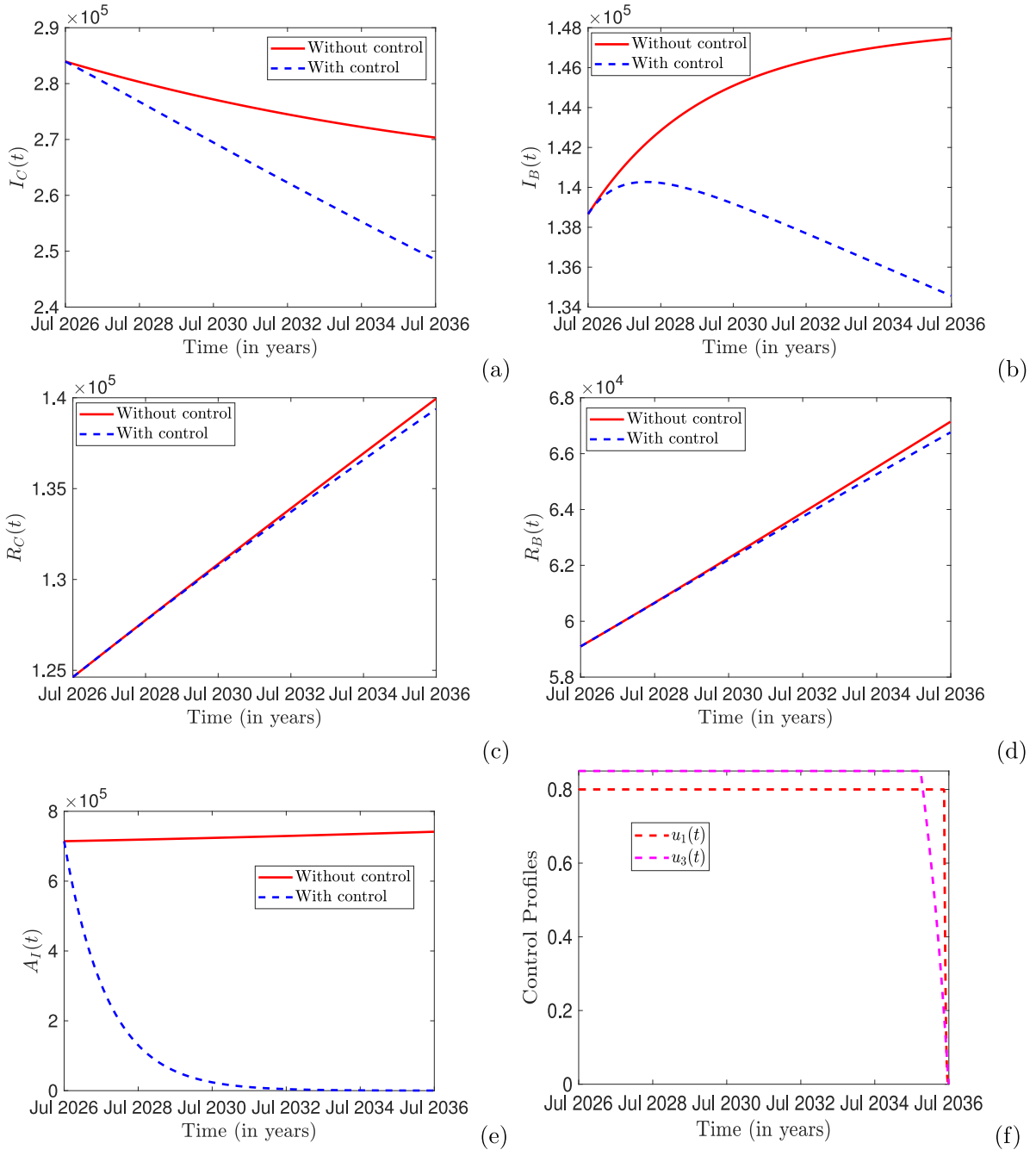

Fig. 9. Simulation results for Strategy C (optimal acaricide application combined with habitat modification) under control bounds $0 \le u_1(t) \le 0.80$ and $0 \le u_3(t) \le 0.85$. Solid red curves represent population levels in the absence of controls, while dashed black curves depict levels when controls are implemented. Panels (a) and (b) show infectious cattle and buffalo populations, respectively; panels (c) and (d) depict carrier cattle and buffalo populations; panel (e) illustrates infectious tick populations; and panel (f) displays the time-varying optimal control rates.

Table 7
Strategies ordered by total infections averted.

Strategy	Infections averted	Total cost
A	17,963	148,075
B	19,049	395,189
C	36,506	689,730
D	36,618	690,110

the cattle population. Similarly, the infectious buffalo population $I_B(t)$, shown in Fig. 10(b), declines progressively under the intervention, reflecting the strategy's effectiveness in reducing infection among buffaloes over the simulation period. Unlike in Fig. 9(c), a pronounced increase in the recovered (carrier) cattle population $R_C(t)$ is observed under the controlled scenario (Fig. 10(c)). The recovered class increases substantially faster compared to the uncontrolled case, highlighting the significant contribution of vaccination in enhancing immunity and recovery among infected cattle. This suggests improved long-term herd protection with the combined intervention, a trend also observed in Fig. 8(c).

Fig. 10(d) shows slight differences between the controlled and uncontrolled trajectories, with the controlled case remaining marginally lower throughout the simulation. This limited variation indicates that these controls exert minimal influence on buffalo dynamics, as the interventions primarily target cattle and tick populations rather than buffalo hosts. In Fig. 10(e), the infected tick population $A_I(t)$ declines rapidly toward near elimination under the control scenario, whereas it remains persistently high in the uncontrolled case. This sharp reduction confirms the effectiveness of combining acaricide application with habitat modification in disrupting tick survival, reproduction, and environmental persistence. The suppression of infected ticks significantly reduces opportunities for disease transmission. The optimal control profiles in Fig. 10(f) show that all three controls — acaricide application $u_1(t)$, vaccination $u_2(t)$, and habitat modification $u_3(t)$ — are maintained at high levels during most of the intervention period, then decline sharply near the end. Notably, habitat modification and vaccination are maintained at slightly higher levels than acaricide application, suggesting their dominant roles in minimizing the objective functional and reducing disease prevalence. The sustained high control efforts underscore the necessity of continuous intervention to achieve long-term suppression of infection and tick populations.

In summary, the integrated approach combining acaricide use, vaccination, and habitat modification yields the greatest epidemiological benefits among the considered strategies. It significantly reduces infections in cattle and buffalo, enhances recovery rates, and nearly eradicates infected tick populations. These findings support the effectiveness and sustainability of a comprehensive control strategy targeting both hosts and vectors for managing East Coast fever in endemic regions.

Cost-effectiveness analysis

To evaluate the economic efficiency of the control measures, we analyze their cost-effectiveness ratios, enabling informed decision-making. This section compares all control strategies (A through E) using three key metrics:

(i) **Average Cost-Effectiveness Ratio (ACER):** The average cost per infection averted, calculated by dividing the net intervention cost by the total infections prevented.
(ii) **Marginal Cost-Effectiveness Ratio (MCER):** The incremental change in cost and effect from modifying a program, providing insight into the cost-effectiveness of small adjustments.
(iii) **Incremental Cost-Effectiveness Ratio (ICER):** The additional cost per additional infection prevented when comparing two strategies, especially useful for selecting among competing options [34,35].

We primarily focus on the ICER, computed as:

$$\text{ICER} = \frac{\text{Difference in total costs}}{\text{Difference in infections averted}}.$$

Total infections averted are obtained by subtracting the number of cases under each control strategy from the baseline (no control). The ICER allows direct comparison of the incremental benefits and costs of strategies, with the less effective option serving as the baseline. A lower ICER indicates better cost-effectiveness. The numerator includes intervention costs, treatment savings, costs avoided from prevented cases, and productivity gains where applicable. The denominator reflects the difference in health outcomes, such as infections prevented. Policymakers can use ICER to allocate resources optimally. Based on our simulation results, the strategies are ranked in order of increasing effectiveness at reducing infections:

- A combination of acaricide use and vaccination (strategy B)
- Acaricide application alone (strategy A)
- A combination of acaricide, vaccination, and habitat modification (strategy D)
- A combination of acaricide and habitat modification (strategy C)

This ranking is summarized in Table 7. The ICERs are calculated as:

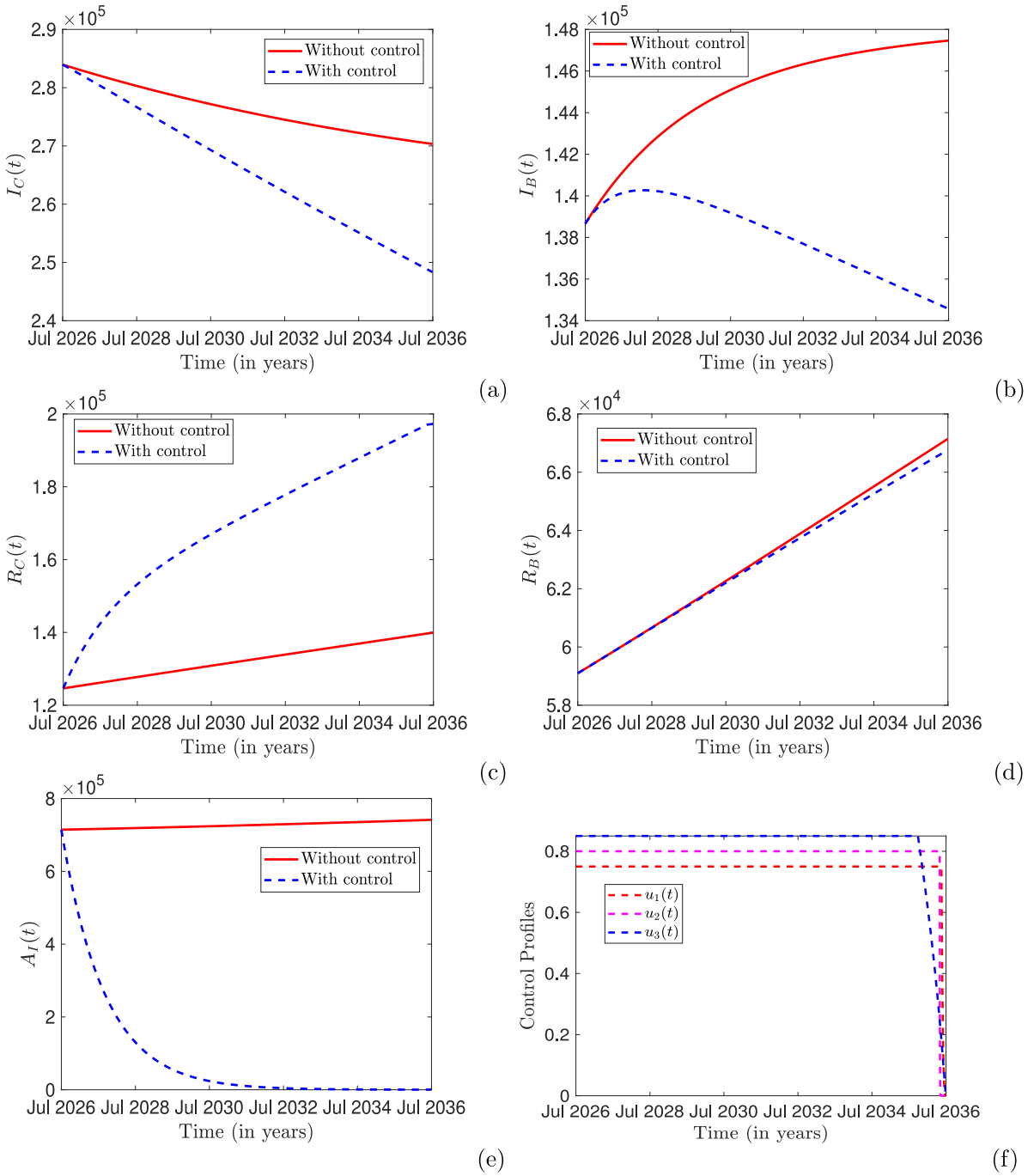

Fig. 10. Simulation results for Strategy D, involving vaccination, acaricide application, and habitat modification, with control bounds $0 < u_1(t) < 0.75$, $0 < u_2(t) \leq 0.80$, and $0 < u_3(t) \leq 0.85$. Solid red curves represent uncontrolled populations; dashed black curves depict controlled populations. Panels (a) and (b) show infectious cattle and buffalo populations, respectively. Panels (c) and (d) display carrier cattle and buffalo populations. Panel (e) depicts infectious tick populations, and panel (f) illustrates the time-varying optimal control rates.

Table 8
ICERs in order of increasing infections averted.

Strategy	Infections averted	Total cost	ICER
A	17,963	148,075	0.1213
C	36,506	689,730	−0.0535
D	36,618	690,110	2.9474

$$\begin{aligned}
\text{ICER (A)} &= \frac{17,963}{148,075} \approx 0.1213,\\
\text{ICER (B)} &= \frac{19,049 - 17,963}{395,189 - 148,075} \approx 0.0044,\\
\text{ICER (C)} &= \frac{36,506 - 19,049}{689,730 - 395,189} \approx -0.0535,\\
\text{ICER (D)} &= \frac{36,618 - 36,506}{690,110 - 689,730} \approx 2.9474.
\end{aligned}$$

From these calculations (see Table 8), strategy B appears less cost-effective relative to strategy A, so we exclude it and compare the remaining strategies:

Next, comparing strategies C and D, the ICER indicates that strategy C is more cost-effective:

$$\begin{aligned}
\text{ICER (C)} &= \frac{36,506 - 19,049}{689,730 - 395,189} \approx -0.0535,\\
\text{ICER (D)} &= \frac{36,618 - 36,506}{690,110 - 689,730} \approx 2.9474.
\end{aligned} \tag{3.3}$$

Since strategy D is more costly and less effective than C (negative ICER), it is dominated and can be excluded. Therefore, the most cost-effective strategies are A and C, with C providing better infection reduction at comparable or slightly higher cost.

4. Concluding remarks and future directions

This study developed a comprehensive mathematical model of East Coast Fever (ECF) transmission at the livestock–wildlife interface, incorporating cattle, buffalo, and tick populations. Calibration with empirical data from Zimbabwe (2014–2020) produced parameter estimates consistent with existing literature and observed disease trends. These calibrations enabled projections up to 2030, which suggest that, under current control practices, ECF incidence may stabilize at a persistent endemic level with minor fluctuations. The model indicates that the basic reproduction number $\mathcal{R}_0$ exceeds 1 in the baseline scenario, confirming the potential for sustained disease transmission without intensified intervention efforts.

Sensitivity analyses identified key parameters influencing $\mathcal{R}_0$, notably tick biting preference (p), transmission probabilities ($\beta_{CT}, \beta_{TC}, \beta_{BT}, \beta_{TB}$), and host and vector recruitment rates (Π_C, Π_B, Π_T). These parameters represent potential targets for control strategies. The optimal control simulations demonstrated that applying acaricides alone can significantly reduce tick populations and infection levels in cattle, but may not achieve complete eradication within a decade. Combining acaricide use with cattle vaccination further decreases infection prevalence, enhances recovery rates, and delays potential disease resurgence. Incorporating habitat modification into control efforts — aimed at reducing environmental tick reservoirs — can markedly accelerate decline in infected vectors and hosts, often approaching elimination thresholds in model simulations. The joint implementation of all three strategies — acaricide application, vaccination, and habitat management — produces the most substantial reductions in infection levels and tick populations, suggesting a synergistic effect that could approximate eradication over an extended period.

Cost-effectiveness analysis indicates that acaricide application alone offers the most economical per-infection averted; however, it may not suffice for complete disease elimination. Adding vaccination improves epidemiological outcomes but entails higher total costs. Strategies combining habitat modification with acaricide and vaccination demonstrate better long-term benefits despite increased operational expenses. Dominance analysis suggests that a combination of acaricide and habitat management (Strategy C) provides a favorable balance of impact and cost, making it an attractive option for sustainable disease control.

Several limitations should be considered. The deterministic nature of the model may overlook stochastic effects, especially in small or fragmented populations, which can influence disease persistence and eradication prospects. Environmental variability and seasonal tick activity were not explicitly modeled, potentially affecting the accuracy of long-term forecasts. Additionally, many parameter estimates were derived from literature and carry inherent uncertainties, which could influence the model's predictive reliability. Socio-economic factors, such as farmer compliance, logistical constraints, and resource availability, were not directly incorporated into the control optimization, limiting the direct applicability of the results.

Future research should focus on incorporating stochastic processes and environmental factors, such as climate variability, to better capture seasonal tick dynamics and their impact on transmission. Integrating climate and habitat data could improve the realism of projections and inform targeted interventions. Refining economic analyses with region-specific costs, including farmer participation and logistical challenges, would enhance policy relevance. Exploring spatially explicit or agent-based modeling approaches to account for the role of wildlife populations and landscape heterogeneity could provide deeper insights into disease persistence. Lastly, engaging stakeholders and policymakers to develop feasible implementation frameworks will be crucial for translating these modeling insights into effective control programs. Overall, the findings underscore that integrated, targeted interventions — tailored to local ecological, economic, and social contexts — are essential for sustainable management of ECF at the livestock–wildlife interface.

CRediT authorship contribution statement

Mirirai Chinyoka: Writing – original draft, Methodology, Formal analysis. **Gift Muchatibaya:** Supervision, Formal analysis. **Mlyashimbi Helikumi:** Formal analysis. **Shingirai T. Murambiwa:** Writing – original draft, Software, Formal analysis. **Prosper Jambwa:** Supervision, Conceptualization. **Steady Mushayabasa:** Writing – review & editing, Supervision, Conceptualization.

Declaration of Generative AI and AI-assisted technologies in the writing process

During the preparation of this work the authors utilized AI to improve language and readability. After using this tool, the authors reviewed and edited the content as needed and take full responsibility for the content of the publication.

Funding

Not applicable.

Declaration of competing interest

The authors declare that they have no known competing financial interests or personal relationships that could have appeared to influence the work reported in this paper.

Acknowledgments

Authors are grateful to anonymous reviewers for their invaluable comments and suggestions, which greatly improved the presentation of this paper. The views, opinions, assumptions or any other information expressed in this article are solely those of the authors.

Appendix A. Bifurcation analysis

Bifurcation analysis reveals how qualitative changes in disease dynamics arise as key epidemiological parameters vary. To perform the general bifurcation theory utilizing the Center Manifold Theorem (CMT) we commence by presenting Theorem A.1 in Castillo-Chavez [23]:

Theorem A.1. *Consider the following general system of ordinary differential equations with parameter ϕ:*

$$\frac{dX}{dt} = f(X, \phi), \ f : \mathbb{R}^n \times \mathbb{R} \to \mathbb{R} \text{ and } f \in C^2(\mathbb{R}^n \times \mathbb{R}). \tag{A.1}$$

Without loss of generality, it is assumed that 0 is an equilibrium for system for all values of the parameter β^*; that is, $f(0, \beta^*) = 0$ for all β^*. Assume

(i) $A = D_x f(0,0) = \left(\frac{\partial f_i}{\partial x_j}(0,0) \right)$ *is the linearization of system around the equilibrium 0 and β^* evaluated at 0. Zero is a simple eigenvalue of A and other eigenvalues of A have negative real parts;*

(ii) Matrix A has the right eigenvector u and a left eigenvector v corresponding to the zero eigenvalue. Let f_k be the kth component of f and

$$a = \sum v_k u_i u_j \frac{\partial^2 f_k(0,0)}{\partial x_i \partial x_j}, \ i, j, k = 1, 2, 3, \dots, n$$

$$b = \sum v_k u_i \frac{\partial^2 f_k(0,0)}{\partial x_i \partial \phi}, \ i, k = 1, 2, 3, \dots, n.$$

The local dynamics of (A.1) around zero are totally governed by a and b.

(i) $a > 0, b > 0$. *When $\phi < 0$ with $\mid \phi \mid \ll 1$, 0 is locally asymptotically stable and there exists a positive unstable equilibrium, when $0 < \phi \ll 1$, 0 is unstable and there exists a negative and locally asymptotically stable equilibrium;*

(ii) $a < 0, b < 0$. *When $\phi < 0$ with $\mid \phi \mid \ll 1$, 0 unstable; when $0 < \phi \ll 1$, 0 is locally asymptotically stable, and there exists a positive unstable equilibrium;*

(iii) $a > 0, b < 0$. *When $\phi < 0$ with $\mid \phi \mid \ll 1$, 0 is unstable, and there exist a locally asymptotically stable negative equilibrium; when $0 < \phi \ll 1$, 0 is stable, and a positive unstable equilibrium appears;*

(iv) $a < 0, b > 0$. *When ϕ changes from negative to positive, 0 changes its stability from stable to unstable. Correspondingly, a negative unstable equilibrium becomes a positive and locally asymptotically stable especially if $a > 0$ and $b > 0$ then backward bifurcation occurs at $\beta^* = 0$.*

Based on Theorem A.1, we redefine the variables of model (2.5) as follows $S_C = x_1, I_C = x_2, R_C = x_3, S_B = x_4, I_B = x_5, R_B = x_6, A_S = x_7, A_I = x_8$. Thus, we rewrite model (2.5) as:

$$\begin{aligned}
\frac{dx_1}{dt} &= f_1 = \Pi_C - (1-p)\delta_C\beta_{TC}x_8x_1 - \mu_C x_1,\\
\frac{dx_2}{dt} &= f_2 = (1-p)\delta_C\beta_{TC}x_8x_1 - (\mu_C + \gamma_C + d_C)x_2,\\
\frac{dx_3}{dt} &= f_3 = \gamma_C x_2 - \mu_C x_3,\\
\frac{dx_4}{dt} &= f_4 = \Pi_B - p\delta_B\beta_{TB}x_8x_4 - \mu_B x_4,\\
\frac{dx_5}{dt} &= f_5 = p\delta_B\beta_{TB}x_5x_8 - (\mu_B + \gamma_B + d_B)x_5,\\
\frac{dx_6}{dt} &= f_6 = \gamma_B x_5 - \mu_B x_6,\\
\frac{dx_7}{dt} &= f_7 = \Pi_T - (1-p)\delta_C\beta_{CT}x_7\left(x_2 + (1-\eta_C)x_3\right)\\
&\quad - p\delta_B\beta_{BT}x_7\left(x_5 + (1-\eta_B)x_6\right) - \mu_A x_7,\\
\frac{dx_8}{dt} &= f_8 = (1-p)\delta_C\beta_{CT}x_7\left(x_2 + (1-\eta_C)x_3\right)\\
&\quad + p\delta_B\beta_{BT}x_7\left(x_5 + (1-\eta_B)x_6\right) - \mu_A x_8.
\end{aligned} \tag{A.2}$$

Linearizing system (A.2) about the DFE yields the following Jacobian matrix:

$$\mathcal{J} = \begin{pmatrix}
-\mu_C & 0 & 0 & 0 & 0 & 0 & 0 & -c_5\\
0 & -z_2 & 0 & 0 & 0 & 0 & 0 & c_5\\
0 & \gamma_C & -\mu_C & 0 & 0 & 0 & 0 & 0\\
0 & 0 & 0 & -\mu_B & 0 & 0 & 0 & -c_6\\
0 & 0 & 0 & 0 & -z_2 & 0 & 0 & c_6\\
0 & 0 & 0 & 0 & \gamma_B & -\mu_B & 0 & 0\\
0 & -c_1 & -c_2 & 0 & -c_3 & -c_4 & \mu_A & 0\\
0 & c_1 & c_2 & 0 & c_3 & c_4 & 0 & -\mu_A
\end{pmatrix},$$

where

$$\begin{aligned}
c_1 &= -\frac{(1-p)\beta_{CT}\Pi_T}{\mu_A}, \qquad c_2 = \frac{(1-p)\beta_{CT}\Pi_T\delta_C(1-\eta_C)}{\mu_A}, \qquad c_3 = -\frac{\beta_{BT}\Pi_T\delta_B}{\mu_A},\\
c_4 &= -\frac{\beta_{BT}\Pi_T\delta_B(1-\eta_B)}{\mu_A}, \qquad c_5 = -\frac{(1-p)\Pi_C\mu_B\mu_A}{\Pi_T((1-p)^2\Pi_C\alpha_1\beta_{CT}\delta_C^2\mu_B + p^2\Pi_B\alpha_2\beta_{BT}\delta_B^2\mu_C)},\\
c_6 &= -\frac{p\Pi_B\delta_B\mu_A\mu_C}{\Pi_T((1-p)^2\Pi_C\alpha_1\beta_{CT}\delta_C^2\mu_B + p^2\Pi_B\alpha_2\beta_{BT}\delta_B^2\mu_C)}
\end{aligned}$$

Choose $\beta_{TC} = \beta_{TB} = \beta^*$ as the bifurcation parameter, then setting $\mathcal{R}_0 = 1$ gives

$$\beta^* = \frac{\mu_A\mu_B\mu_C}{(1-p)^2\Pi_C\Pi_T\alpha_1\beta_{CT}\delta_C^2\mu_B + p^2\Pi_B\Pi_T\alpha_2\beta_{BT}\delta_B^2\mu_C} \tag{A.3}$$

where

$$\alpha_1 = \frac{1}{a_1} + \frac{(1-\eta_C)\gamma_C}{a_1\mu_C}, \qquad \alpha_2 = \frac{1}{a_2} + \frac{(1-\eta_B)\gamma_B}{a_2\mu_B}.$$

We now proceed to determine the simple zero eigenvalue for $D_x f(x_0, \phi)|_{\mathcal{R}_0=1}$, and the corresponding left and right eigenvectors $\mathbf{v}$ and $\mathbf{u}$, such that $\mathbf{vu} = 1$. Making use of matrix $\mathcal{J}$, the corresponding expression for $\mathbf{u}$ and $\mathbf{v}$ given by:

$$\begin{aligned}
u_1 &= \frac{c_5z_1(c_4u_5\gamma_B + c_3u_5\mu_B)}{\mu_B(c_2c_5\gamma_C + c_1c_5\mu_C - z_1\mu_A\mu_C)}, \qquad u_2 = -\frac{c_5(c_4u_5\gamma_B\mu_C + c_3u_5\mu_B\mu_C)}{\mu_B(c_2c_5\gamma_C + c_1c_5\mu_C - z_1\mu_A\mu_C)},\\
u_3 &= -\frac{c_5\gamma_C(c_4u_5\gamma_B + c_3u_5\mu_B)}{\mu_B(c_2c_5\gamma_C + c_1c_5\mu_C - z_1\mu_A\mu_C)}, \qquad u_4 = \frac{c_6z_1(c_4u_5\gamma_B\mu_C + c_3u_5\mu_B\mu_C)}{\mu_B^2(c_2c_5\gamma_C + c_1c_5\mu_C - z_1\mu_A\mu_C)},\\
u_5 &= u_5 > 0, \qquad u_6 = \frac{u_5\gamma_B}{\mu_B}, \qquad u_7 = \frac{(c_5u_5z_1\gamma_B\mu_C + c_3u_5\mu_B\mu_C)}{\mu_B(c_2c_5\gamma_C + c_1c_5\mu_C - z_1\mu_A\mu_C)},\\
u_8 &= \frac{z_1(c_4u_5\gamma_B\mu_C + c_3u_5\mu_B\mu_C)}{\mu_B(c_2c_5\gamma_C + c_1c_5\mu_C - z_1\mu_A\mu_C)}.
\end{aligned}$$

Similarly, the non-zero left eigenvector are

$$v_1 = v_1 = 0, \qquad v_2 = -\frac{c_6 v_5(c_2\gamma_C + c_1\mu_C)}{c_2c_5\gamma_C + c_1c_5\mu_C - z_1\mu_A\mu_C}, \qquad v_3 = -\frac{c_2c_6v_5z_1}{c_2c_5\gamma_C + c_1c_5\mu_C - z_1\mu_A\mu_C},$$
$$v_4 = v_4 = 0, \qquad v_5 = v_5 > 0, \qquad v_6 = -\frac{c_4c_6v_5z_1\mu_C}{\mu_B(c_2c_5\gamma_C + c_1c_5\mu_C - z_1\mu_A\mu_C)}, \qquad v_7 = v_7 = 0,$$
$$v_8 = -\frac{c_6v_5z_1\mu_C}{\mu_B(c_2c_5\gamma_C + c_1c_5\mu_C - z_1\mu_A\mu_C)}.$$

Next, we determine the second-order partial derivatives of f for

$$\frac{\partial^2 f_i(x_0,\phi)}{\partial x_j\partial x_k}|_{\mathcal{R}_0=1}, \qquad \text{and} \qquad \frac{\partial^2 f_i(x_0,\phi)}{\partial x_j\partial\beta}|_{\mathcal{R}_0=1}.$$

One can easily verify that the non-zero elements second-order partial derivatives of f are:

$$\frac{\partial^2 f_1}{\partial x_1\partial x_8} = \frac{\partial^2 f_1}{\partial x_8\partial x_1} = -((1-p)\beta\delta_C), \qquad \frac{\partial^2 f_2}{\partial x_2\partial x_8} = \frac{\partial^2 f_2}{\partial x_8\partial x_2} = -(1-p)\beta\delta_C,$$
$$\frac{\partial^2 f_4}{\partial x_4\partial x_8} = \frac{\partial^2 f_4}{\partial x_8\partial x_4} = -p\beta\delta_B, \qquad \frac{\partial^2 f_5}{\partial x_5\partial x_8} = \frac{\partial^2 f_5}{\partial x_8\partial x_5} = p\beta\delta_B,$$
$$\frac{\partial^2 f_7}{\partial x_2\partial x_7} = \frac{\partial^2 f_7}{\partial x_7\partial x_2} = -(1-p)\beta_{CT}, \qquad \frac{\partial^2 f_7}{\partial x_3\partial x_7} = \frac{\partial^2 f_7}{\partial x_7\partial x_3} = -(1-p)\beta_{TC}(1-\eta_C),$$
$$\frac{\partial^2 f_7}{\partial x_5\partial x_7} = \frac{\partial^2 f_7}{\partial x_7\partial x_5} = -p\beta_{BT}, \qquad \frac{\partial^2 f_7}{\partial x_6\partial x_7} = \frac{\partial^2 f_7}{\partial x_6\partial x_7} = p\beta_{BT}(1-\eta_B),$$
$$\frac{\partial^2 f_8}{\partial x_2\partial x_7} = \frac{\partial^2 f_8}{\partial x_7\partial x_2} = (1-p)\beta_{CT}, \qquad \frac{\partial^2 f_8}{\partial x_3\partial x_7} = \frac{\partial^2 f_8}{\partial x_7\partial x_3} = (1-p)\beta_{CT}(1-\eta_C),$$
$$\frac{\partial^2 f_8}{\partial x_5\partial x_7} = \frac{\partial^2 f_8}{\partial x_7\partial x_5} = p\beta_{BT}, \qquad \frac{\partial^2 f_8}{\partial x_6\partial x_7} = \frac{\partial^2 f_8}{\partial x_7\partial x_6} = p\beta_{BT}(1-\eta_B).$$

The associated bifurcation coefficients defined by a and b are given by the following equations respectively:

$$\begin{aligned} a &= \sum_{k,i,j=1}^{n} v_k u_i u_j \frac{\partial^2 f_k}{\partial x_i\partial x_j}(0,0), \\ &= v_1u_1u_8(-(1-p)\beta\delta_C) + v_2u_2u_8(-(1-p)\beta\delta_C) + v_4u_4u_8(-p\delta_C\beta) + v_5u_4u_8(-p\delta_C\beta) \\ &\quad + v_7u_2u_7(-(1-p)\beta_{CT}) + v_7u_3u_7(-(1-p)\beta_{CT}(1-\eta_C)) + v_7u_5u_7(-p\beta_{BT}) + v_7u_6u_7(p\beta_{BT}(1-\eta_B)) \\ &\quad + v_8u_2u_7((1-p)\beta_{CT}) + v_8u_3u_7((1-p)\beta_{CT}(1-\eta_C)) + v_8u_5u_7(p\beta_{BT}) \\ &\quad + v_8u_6u_7(p\beta_{BT}(1-\eta_B)) < 0. \end{aligned}$$

Similarly, it follows that

$$\begin{aligned} b &= \sum_{k,i=1}^{n} v_k u_i \frac{\partial^2 f_k}{\partial x_i\partial\beta}(0,0). \\ &= v_1u_1\left(\frac{(1-p)\Pi_C\delta_C}{\mu_C}\right) + v_2u_2\left(\frac{(1-p)\Pi_C\delta_C}{\mu_C}\right) + v_4u_4\left(\frac{-p\Pi_B\delta_B}{\mu_B}\right) + v_5u_5\left(\frac{p\Pi_B\delta_B}{\mu_B}\right) > 0. \end{aligned}$$

Since $a \le 0$ and $b > 0$ it follows that model equations (2.5) admits a forward bifurcation at $\mathcal{R}_0 = 1$. This completes Theorem 2.3.

To support the claim in Theorem 2.3 we simulated model (2.5) using parameter values in Table 5 and obtained the results in Figure refbif1 which illustrates the existence of a forward bifurcation.

Fig. 11 illustrates the bifurcation behavior of the model with respect to the tick-to-cattle transmission rate β_{TC}. The plot shows a forward bifurcation, where the steady-state number of infected cattle I_C^* remains near zero for low values of β_{TC} and increases rapidly beyond a critical threshold. This indicates that reducing β_{TC} below this threshold can eliminate endemic infection, highlighting the importance of controlling tick transmission to cattle.

Appendix B. Necessary conditions for the optimality

The optimal control problem (2.12) can be reduced to minimizing the corresponding Hamiltonian with respect to u_1, u_2 and u_3

$$\mathcal{H}(t,\mathbf{x},\mathbf{u},\lambda) = A_1I_C(t) + A_2R_C + A_3N_T + \frac{1}{2}w_1u_1^2(t) + \frac{1}{2}w_2u_2^2(t) + \frac{1}{2}w_3u_3^2 + \lambda_k f_k,$$

where $\lambda = [\lambda_1(t), \lambda_2(t), \dots, \lambda_8(t)]$ are the adjoint variable for a 8 dimensional state, that is., $\mathbf{x} = (S_C,\ I_C,\ R_C,\ S_B,\ I_B,\ R_B,\ A_S,\ A_I)$, $\mathbf{u} = (u_1, u_2, u_3)$, and f_k is the right hand side of model (2.12) with $k = 1, 2, \dots, 8$. The Hamiltonian is constructed to satisfy the first

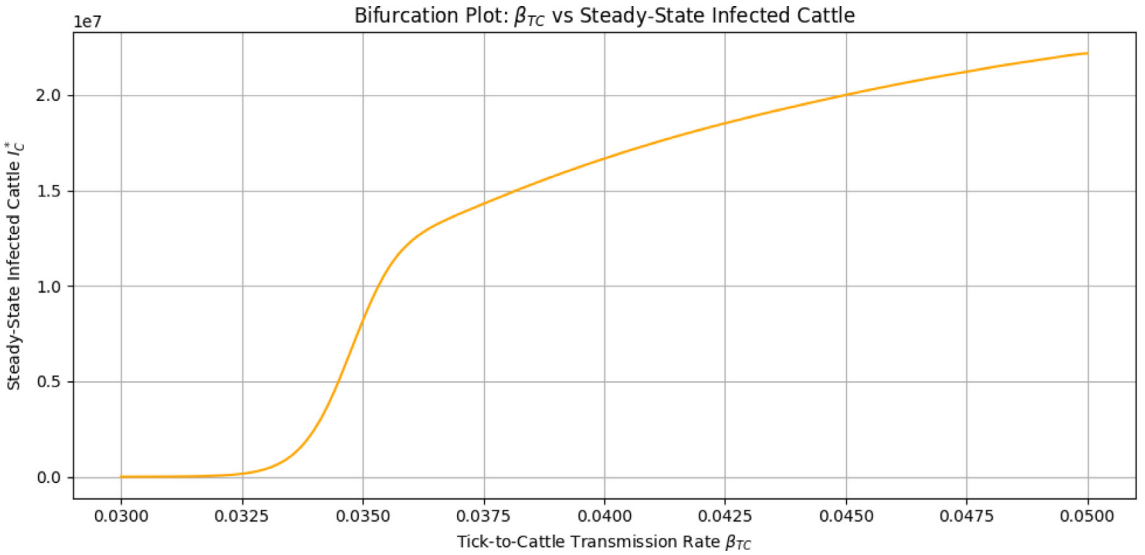

Fig. 11. Bifurcation Plot: Effect of the tick-to-cattle transmission rate β_{TC} on the steady-state number of infected cattle I_C^*. A forward bifurcation is observed, indicating a critical threshold of β_{TC} beyond which endemic infection persists.

the following relation $\frac{\partial \mathcal{H}}{\partial \mathbf{x}} = -\frac{d\lambda}{dt}$, that is:

$$
\begin{aligned}
\dot{\lambda}_1(t) &= -(1-p)A_I(1-u_1(t))\delta_C\beta_{TC}(\lambda_1-\lambda_2) + u_2(t)(\lambda_3-\lambda_1) - \lambda_1\mu_C,\\
\dot{\lambda}_2(t) &= A_1 - \lambda_2(\mu_C+\gamma_C+d_C) + \gamma_C\lambda_3 + A_S\delta_C\beta_{CT}(\lambda_8-\lambda_7) + pA_S\delta_C\beta_{CT}(\lambda_7-\lambda_8)\\
&\quad + A_S u_1(t)\delta_C\beta_{CT}(\lambda_7-\lambda_8) + pA_S u_1(t)\delta_C\beta_{CT}(\lambda_8-\lambda_7),\\
\dot{\lambda}_3(t) &= A_2 + (1-p)A_S(1-u_1(t))\delta_C\beta_{CT}(1-\eta_C)(\lambda_7-\lambda_8) - \lambda_3\mu_C,\\
\dot{\lambda}_4(t) &= pA_I\delta_B\beta_{TB}(\lambda_5-\lambda_4) - \mu_B\lambda_4,\\
\dot{\lambda}_5(t) &= -\lambda_5(\mu_B+d_B) + \gamma_B(\lambda_6-\lambda_5) + pA_S\delta_B\beta_{BT}(\lambda_8-\lambda_7),\\
\dot{\lambda}_6(t) &= pA_S\delta_B\beta_{TB}(1-\eta_B)(\lambda_7-\lambda_8) - \mu_B\lambda_6\\
\dot{\lambda}_7(t) &= A_3 + pR_B\delta_B\beta_{BT}(\lambda_8-\lambda_7) + I_C\delta_C\beta_{CT}(\lambda_8-\lambda_7) + R_C\delta_C\beta_{CT}\eta_C(\lambda_7-\lambda_8)\\
&\quad + pI_C\delta_C\beta_{CT}(\lambda_7-\lambda_8) + pR_C\delta_C\beta_{CT}\eta_C(\lambda_8-\lambda_7) + R_C\delta_C\beta_{CT}(\lambda_8-\lambda_7)\\
&\quad + R_C u_1(t)\delta_C\beta_{CT}\eta_C(\lambda_8-\lambda_7) + pR_C\delta_C\beta_{CT}(\lambda_7-\lambda_8) + pR_C u_1(t)\delta_C\beta_{CT}\eta_C(\lambda_7-\lambda_8)\\
&\quad + I_C u_1(t)\delta_C\beta_{CT}(\lambda_7-\lambda_8) + pI_C u_1(t)\delta_C\beta_{CT}(\lambda_8-\lambda_7) + R_C u_1(t)\delta_C\beta_{CT}(\lambda_7-\lambda_8)\\
&\quad + pR_C u_1(t)\delta_C\beta_{CT}(\lambda_8-\lambda_7) + pR_B\delta_B\beta_{BT}\eta_B(\lambda_7-\lambda_8)\\
&\quad + pI_B\delta_B\beta_{BT}(\lambda_8-\lambda_7) - \lambda_7(\mu_A+u_3(t)),\\
\dot{\lambda}_8(t) &= A_3 + (1-p)S_C(1-u_1(t))\delta_C\beta_{TC}(\lambda_1-\lambda_2) + pS_B\delta_B\beta_{BT}(\lambda_5-\lambda_4) - \lambda_8(\mu_A+u_3(t)).
\end{aligned}
\tag{B.1}
$$

Furthermore, the optimality condition is determined by minimizing the Hamiltonian $\frac{\partial \mathcal{H}}{\partial \mathbf{u}} = 0$. Thus, the optimal controls are characterized by:

$$
\begin{aligned}
u_1^\star &= \max\left\{0, \min\left\{\frac{1, (-((1-p)\delta_C(A_I S_C\beta_{TC}(\lambda_1-\lambda_2))) + A_S\beta_{CT}(I_C - R_C(1-\eta_C)(\lambda_7-\lambda_8)))}{w_1}\right\}\right\},\\
u_2^\star &= \max\left\{0, \min\left\{1, \frac{S_C(\lambda_1-\lambda_3)}{w_2}\right\}\right\},\\
u_3^\star &= \max\left\{0, \min\left\{1, \frac{(A_S\lambda_7 + A_I\lambda_8)}{w_3}\right\}\right\}.
\end{aligned}
\tag{B.2}
$$

In (B.2), $u_{1}\max \le 1$, $u_{2}\max \le 1$, and $u_{3}\max \le 1$ are the feasible upper bounds of the controls $u_1(t)$, $u_2(t)$ and $u_3(t)$, respectively.

Data availability

All the datasets used as well as generated in this study are included in the manuscript.

References

[1] Morrison W Ivan, Hemmink Johanneke D, Toye Philip G. Theileria parva: a parasite of African buffalo, which has adapted to infect and undergo transmission in cattle. Int J Parasitol 2020;50(5):403–12. http://dx.doi.org/10.1016/j.ijpara.2019.12.006.

[2] Nicholson William L, et al. Ticks (ixodida). Med Vet Entomol. 2019;50:603–72. http://dx.doi.org/10.1016/B978-0-12-814043-7.00027-3.

[3] Walker JG, Klein EY, Levin SA. Disease at the wildlife-livestock interface: acaricide use on domestic cattle does not prevent transmission of a tick-borne pathogen with multiple hosts. Vet Parasitol 2014;199(3–4):206–14. http://dx.doi.org/10.1016/j.vetpar.2013.11.008.

[4] Atuhaire David Kalenzi, et al. Molecular characterization and population genetics of *Theileria parva* in Burundi's unvaccinated cattle: Towards the introduction of East Coast fever vaccine. PLoS One 2021;16(5):e0251500. http://dx.doi.org/10.1371/journal.pone.0251500.

[5] Maboko Boitumelo B, et al. South African buffalo-derived *Theileria parva* is distinct from other buffalo and cattle-derived. T Parva. Front. Genet. 2021;12:666096. http://dx.doi.org/10.3389/fgene.2021.666096.

[6] Nanteza Anne, et al. Antigen gene and variable number tandem repeat (VNTR) diversity in *Theileria parva* parasites from Ankole cattle in south-western Uganda: Evidence for conservation in antigen gene sequences combined with extensive polymorphism at VNTR loci. Transbound Emerg Dis 2020;67:99–107. http://dx.doi.org/10.1111/tbed.13311.

[7] Nene V, Kiara H, Lacasta A, Pelle R, Svitek N, Steinaa L. The biology of *Theileria parva* and control of East Coast fever—current status and future trends. Ticks Tick Borne Dis 2016;7:549–64. http://dx.doi.org/10.1016/j.ttbdis.2016.02.001.

[8] Chinyoka M, Muchatibaya G, Jambwa P, Masocha M, Mushayabasa S. Assessing the potential impact of livestock immunisation and acaricide use on controlling the spread of East Coast fever. Parasite Epidemiol Control 2024;25:e00357. http://dx.doi.org/10.1016/j.parepi.2024.e00357.

[9] Barasona JA, Latham MC, Acevedo P, Armenteros JA, Latham ADM, Gortazar C, Carro F, Soriguer RC, Vicente J. Spatiotemporal interactions between wild boar and cattle: implications for cross-species disease transmission. Vet Res 2014;45:1–11. http://dx.doi.org/10.1186/s13567-014-0122-7.

[10] Gilioli G, Groppi M, Vesperoni MP, Baumgärtner J, Gutierrez AP. An epidemiological model of East Coast Fever in African livestock. Ecol Model 2009;220:1652–62. http://dx.doi.org/10.1016/j.ecolmodel.2009.03.017.

[11] O'Callaghan CJ, Medley GF, Peter TF, Perry BD. Investigating the epidemiology of heartwater (Cowdria ruminantium infection) by means of a transmission dynamics model. Parasitol 1998;117(1):49–61. http://dx.doi.org/10.1017/S0031182098002790.

[12] Medley GF, Perry BD, Young AS. Preliminary analysis of the transmission dynamics of *Theileria parva,* in eastern Africa. Parasitology 1993;106(3):251–64. http://dx.doi.org/10.1017/S0031182000075077.

[13] Mwambi HG, Baumgärtner J, Hadeler KP. Ticks and tick-borne diseases: a vector-host interaction model for the brown ear tick (*Rhipicephalus appendiculatus*). Stat Methods Med Res 2000;9(3):279–301. http://dx.doi.org/10.1177/0962280200009003.

[14] Ugirabe MA, NjiAbatih E, Berkvens ID. A differential equations model of east coast fever transmission dynamics. Rwanda J Agric Sci 2019;1(1):36–43, https://www.ajol.info/index.php/rjeas/article/view/193255.

[15] Tardy O, Acheson ES, Bouchard C, Chamberland E, Fortin A, Ogden NH, Leighton PA. Mechanistic movement models to predict geographic range expansions of ticks and tick-borne pathogens: Case studies with *Ixodes scapularis* and *Amblyomma americanum* in eastern North America. Ticks Tick Borne Dis 2023;14(4):102161. http://dx.doi.org/10.1016/j.ttbdis.2023.102161.

[16] Ikaal MA, Kashongwe OB, Bebe BO. Prevalence of East Coast fever infections based on farmer-observed symptoms in smallholder dairy herds, North Rift Kenya. Int J Vet Sci Anim. Husb 2020;5(2):22–8. http://dx.doi.org/10.22271/veterinary.

[17] Mukandabvute D, Paul NH, Songwe F. Theileria parva genetics, prevalence and vaccination practices in zimbabwe and the african region and the prospects for vaccine development: a systematic review. Vet Res Commun 2025;49:146. http://dx.doi.org/10.1007/s11259-025-10715-x.

[18] Nhokwara SM, Kono H, Kubota S, Jubenkanda M. Communication medium in theileriosis control: the factors that determine disease knowledge among smallholder farmers in Zimbabwe. Trop Anim Health Prod 2023;55(2):83. http://dx.doi.org/10.1007/s11250-023-03466-x.

[19] Igoe M, Casagrandi R, Gatto M, Hoover CM, Mari L, Ngonghala CN, Remais JV, Sanchirico JN, Sokolow S, Lenhart S. Reframing optimal control problems for infectious disease management in low-income countries. Bull Math Biol 2023;85(4):31. http://dx.doi.org/10.1007/s11538-023-01137-4.

[20] Diekmann O, Heesterbeek JAP, Roberts MG. The construction of next-generation matrices for compartmental epidemic models. J R. Soc Interface 2010;7(47):873–85. http://dx.doi.org/10.1098/rsif.2009.0386.

[21] Van den Driessche P, Watmough J. Reproduction numbers and sub-threshold endemic equilibria for compartmental models of disease transmission. Math Biosci Eng 2002;180(1–2):29–48. http://dx.doi.org/10.1016/S0025-5564(02)00108-6.

[22] Castillo-Chavez C, Blower S, Van den Driessche P, Kirschner D, Yakubu AA. Mathematical approaches for emerging and reemerging infectious diseases: Models, methods, and theory. New York: Springer; 2002, http://dx.doi.org/10.1007/978-1-4613-0065-6.

[23] Castillo-Chavez C, Song B. Dynamical models of tuberculosis and their applications. Math Biosci Eng 2004;1(4):361–404. http://dx.doi.org/10.3934/mbe.2004.1.361.

[24] Helikumi M, Daudi S, Lusekelo E, Mushayabasa S. Optimizing combination therapy against drug resistance Mycobacterium tuberculosis: a modelling study. J Biol Phys 2025;51(1):20. http://dx.doi.org/10.1007/s10867-025-09685-7.

[25] Pontryagin LS. Mathematical theory of optimal processes. Routledge; 2018, http://dx.doi.org/10.1201/9780203749319.

[26] Sharp JA, Browning AP, Mapder T, Burrage K, Simpson MJ. Optimal control of acute myeloid leukaemia. J Theoret Biol 2019;470:30–42. http://dx.doi.org/10.1016/j.jtbi.2019.03.006.

[27] Keeling Matt J, Rohani Pejman. Modeling infectious diseases in humans and animals. Princeton University Press; 2008.

[28] Chowell Gerardo. Fitting dynamic models to epidemic outbreaks with quantified uncertainty: A primer for parameter uncertainty, identifiability, and forecasts. Infect Dis Model 2017;2(3):379–98. http://dx.doi.org/10.1016/j.idm.2017.08.00.

[29] Zimbabwe integrated tick and tick-borne disease control strategy 2022–2030. 2024, Available at: https://zagp.org.zw/Content/recource_center_files/30731b3d-7b21-4a0a-a41c-3a25a23adf80.pdf. [Accessed 3 July 2024].

[30] Asamoah JKK. A fractional mathematical model of heartwater transmission dynamics considering nymph and adult amblyomma ticks. Chaos Solitons Fractals 2023;174:113905. http://dx.doi.org/10.1016/j.chaos.2023.113905.

[31] Marino S, Hogue IB, Ray CJ, Kirschner DE. A methodology for performing global uncertainty and sensitivity analysis in systems biology. J Theoret Biol 2008;254(1):178–96. http://dx.doi.org/10.1016/j.jtbi.2008.04.011.

[32] Lenhart S, Workman JT. Optimal control applied to biological models. Chapman & Hall/CRC; 2007, http://dx.doi.org/10.1201/9781420011418.

[33] D'haese L, Penne K, Elyn R. Economics of theileriosis control in Zambia. Trop Med Int Health 1999;4(9):A49–57. http://dx.doi.org/10.1046/j.1365-3156.1999.00451.x.

[34] Agusto FB, Leite MCA. Optimal control and cost-effective analysis of the 2017 meningitis outbreak in Nigeria. Infect Dis Model 2019;4:161–87. http://dx.doi.org/10.1016/j.idm.2019.05.003.

[35] Okosun K, Ouifki R, Marcus N. Optimal control analysis of a malaria disease transmission model that includes treatment and vaccination with waning immunity. Biosystems 2011;106(2–3):136–45. http://dx.doi.org/10.1016/j.biosystems.2011.07.006.